

Measurement and Analysis of Electric Fields in Ocean Environments

A Thesis

Presented in Partial Fulfillment of the Requirements for the

Degree of Master of Science

with a

Major in Mechanical Engineering

in the

College of Graduate Studies

University of Idaho

by

Ronnie Lee Ross

Major Professor: Michael Anderson, Ph.D.

Committee Members: Eric Wolbrecht, Ph.D.; Dean Edwards, Ph.D.

Department Administrator: Steven Beyerlein, Ph.D.

May 2017

Authorization to Submit Thesis

This thesis of Ronnie Lee Ross, submitted for the degree of Master of Science with a major in Mechanical Engineering and titled “Measurement and Analysis of Electric Fields in Ocean Environments,” has been reviewed in final form. Permission, as indicated by the signatures and dates below, is now granted to submit final copies to the College of Graduate Studies for approval.

Major Professor: _____ Date: _____
Michael Anderson, Ph.D.

Committee Members: _____ Date: _____
Eric Wolbrecht, Ph.D.

Dean Edwards, Ph.D. Date: _____

Department
Administrator: _____ Date: _____
Steven Beyerlein, Ph.D.

Abstract

The University of Idaho (UI) worked with the Office of Naval Research (ONR) to develop a sensor system that could be attached to an Autonomous Underwater Vehicle (AUV) to make magnetic and electric field measurements in the ocean. This thesis presents the use of the electric field sensor and the process of analyzing measurements taken with it. The sensors were created at the UI and electrodes were used to measure the generated electric fields that were placed in test environments. Measurements of these fields were compared to prediction models to determine the accuracy of the sensors. The measured electric field was bounded by a prediction of the free space model and the model that includes the boundary effects. An example peak of the measured electric field was 7,000 $\mu\text{V}/\text{m}$ which was between the bounds of the model at 11,000 $\mu\text{V}/\text{m}$ and 2,000 $\mu\text{V}/\text{m}$. The RMS values of the noise floor, $\sim 1 \mu\text{V}/\text{m}$, were within the target range of ONR's specifications and further analysis into how to improve the sensors was being conducted. One area of future improvement that was investigated was the navigation accuracy of the AUV. There was evidence that shows with improved accuracy of the AUV position data, the electric field measurements could also be improved.

Acknowledgements

I would like to thank my major professor, Dr. Michael Anderson, for his advice, help, and expertise during this research. I would also like to thank my committee, Dr. Dean Edwards and Dr. Wolbrecht, for their work on this project. I would like to thank the other graduate, undergraduate, and faculty members who have worked on this project and have been instrumental in the success of this research. Lastly, I would like to thank The Office of Naval Research for their support and funding of this project.

Table of Contents

Authorization to Submit Thesis	ii
Abstract	iii
Acknowledgements	iv
Table of Contents	v
List of Figures	vii
Chapter 1: Introduction	1
1.1 Project Overview	1
1.2 Current State of the Project	2
Chapter 2: Methods	4
2.1 Testing Strategy and Overview	4
2.2 Sensors	4
2.3 Dealing with Electrode Drift in Post Processing	6
2.4 Electric Field Modeling	10
2.5 Noise Floor Measurements in the Lab	14
2.6 Lab Testing Apparatus and Process	14
2.6.1 - Response to a Controlled Electric Field Source	16
2.6.2 - Signal Analysis	16
2.7 Field Testing	17
2.7.1 - ARD at Bayview	17
2.7.2 - Florida: April 2016	17
2.7.3 - Florida: August 2016	19
Chapter 3: Results & Discussion	21
3.1 Measurement and Analysis of Signals	21
3.1.1 - Lab Testing of Electric Field Sensors	21

3.1.2 - Tests Taken Along Pier at SFOMC	25
3.1.3 - SFOMC Offshore Tests.....	32
3.1.4 - Sensitivity Analysis.....	42
Chapter 4: Conclusions and Future Work.....	45
4.1 Conclusions	45
4.2 Future Work	46
References.....	47
Appendix A: August 2016 SFOMC Tests	48

List of Figures

Figure 2.1: 3 inch sensor with embedded electrodes and preamplifier	5
Figure 2.2: Measured electric field from Sub 7 Run 38 from Florida on August 17, 2016. 7	7
Figure 2.3: Measured electric field from Sub 7 Run 12 from Florida on August 19, 2016. 7	7
Figure 2.4: Electric field measurement with a cubic polynomial fit.....	9
Figure 2.5: Electric field measurement after the polynomial fit is removed	9
Figure 2.6: A representation of reflections from boundary effects	10
Figure 2.7: Visualization of electric field created by source boat during Florida ocean tests	13
Figure 2.8: Lab set up for testing electric field sensors	15
Figure 2.9: Faraday cage in lab	16
Figure 2.10: Copper plate used to create desired electric fields	19
Figure 2.11: AUV off the pier at SFOMC	19
Figure 3.1: Amplitude spectral density of 3.81cm (1.5”) diameter probe with cylindrical electrodes (preamp outside probe)	22
Figure 3.2: Amplitude spectral density of 7.2cm (3”) diameter probe with cylindrical electrodes (preamp inside probe)	22
Figure 3.3: Amplitude spectral density of 7.2cm (3”) diameter probe with disk electrodes (preamp inside probe)	23
Figure 3.4: Amplitude spectral density for a tank test with a 10 Hz signal in the water ...	24
Figure 3.5: Electric field measurement of ambient field pier side.....	25
Figure 3.6: Amplitude spectral density of ambient field measurement pier side.....	26
Figure 3.7: Electric field measurement of 1 Hz source signal pier side	27

Figure 3.8: Amplitude spectral density of 1 Hz source signal pier side	28
Figure 3.9: Electric field measurement of 10 Hz source signal pier side	29
Figure 3.10: Amplitude spectral density of 10 Hz source signal pier side	29
Figure 3.11: Electric field measurement of DC signal pier side	30
Figure 3.12: Amplitude spectral density of DC signal pier side	31
Figure 3.13: Position, depth, and closest pass of AUV and Parker for AUV 7 run 38 on Wednesday, August 17, 2016	33
Figure 3.14: Magnitude of measured electric field for AUV 7 Run 38 Wednesday, August 17, 2016.....	33
Figure 3.15: Zoomed in view of the magnitude of the measured signal from the source boat	34
Figure 3.16: Position, depth, and closest pass of AUV and Parker for AUV 7 run 29 on Wednesday, August 17, 2016	35
Figure 3.17: Magnitude of measured electric field for AUV 7 Run 29 Wednesday, August 17, 2016.....	36
Figure 3.18: Zoomed in view of the magnitude of the measured signal from the source boat	36
Figure 3.19: Position, depth, and closest pass of AUV and Parker for AUV 7 run 12 on Friday, August 19, 2016.....	37
Figure 3.20: Magnitude of measured electric field for AUV 7 Run 12 Friday, August 19, 2016.....	38
Figure 3.21: Zoomed in view of the magnitude of the measured signal from the source boat	38

Figure 3.22: Position, depth, and closest pass of AUV and Parker for AUV 7 run 81 on Friday, August 19, 2016.....	39
Figure 3.23: Magnitude of measured electric field for AUV 7 Run 81 Friday, August 19, 2016.....	40
Figure 3.24: Variation of AUV position	42
Figure 3.25: Evaluation of the sensitivity of the AUV position data on the theoretical electric field	43
Figure 3.26: Zoomed in view of sensitivity variation	43
Figure A.1: Position, depth, and closest pass of AUV and Parker for AUV 7 run 36 on Wednesday, August 17, 2016	48
Figure A.2: Magnitude of measured electric field for AUV 7 Run 26 Wednesday, August 17, 2016.....	48
Figure A.3: Position, depth, and closest pass of AUV and Parker for AUV 7 run 03 on Friday, August 19, 2016.....	49
Figure A.4: Magnitude of measured electric field for AUV 7 Run 03 Friday, August 19, 2016.....	49
Figure A.5: Position, depth, and closest pass of AUV and Parker for AUV 7 run 06 on Friday, August 19, 2016.....	50
Figure A.6: Magnitude of measured electric field for AUV 7 Run 06 Friday, August 19, 2016.....	50
Figure A.7: Position, depth, and closest pass of AUV and Parker for AUV 7 run 09 on Friday, August 19, 2016.....	51

Figure A.8: Magnitude of measured electric field for AUV 7 Run 09 Friday, August 19, 2016.....	51
Figure A.9: Position, depth, and closest pass of AUV and Parker for AUV 7 run 16 on Friday, August 19, 2016.....	52
Figure A.10: Magnitude of measured electric field for AUV 7 Run 16 Friday, August 19, 2016.....	52
Figure A.11: Position, depth, and closest pass of AUV and Parker for AUV 7 run 19 on Friday, August 19, 2016.....	53
Figure A.12: Magnitude of measured electric field for AUV 7 Run 19 Friday, August 19, 2016.....	53
Figure A.13: Position, depth, and closest pass of AUV and Parker for AUV 7 run 22 on Friday, August 19, 2016.....	54
Figure A.14: Magnitude of measured electric field for AUV 7 Run 22 Friday, August 19, 2016.....	54
Figure A.15: Position, depth, and closest pass of AUV and Parker for AUV 7 run 25 on Friday, August 19, 2016.....	55
Figure A.16: Magnitude of measured electric field for AUV 7 Run 25 Friday, August 19, 2016.....	55
Figure A.17: Position, depth, and closest pass of AUV and Parker for AUV 7 run 31 on Friday, August 19, 2016.....	56
Figure A.18: Magnitude of measured electric field for AUV 7 Run 31 Friday, August 19, 2016.....	56

Figure A.19: Position, depth, and closest pass of AUV and Parker for AUV 7 run 73 on Friday, August 19, 2016.....	57
Figure A.20: Magnitude of measured electric field for AUV 7 Run 73 Friday, August 19, 2016.....	57
Figure A.21: Position, depth, and closest pass of AUV and Parker for AUV 7 run 75 on Friday, August 19, 2016.....	58
Figure A.22: Magnitude of measured electric field for AUV 7 Run 75 Friday, August 19, 2016.....	58
Figure A.23: Position, depth, and closest pass of AUV and Parker for AUV 7 run 79 on Friday, August 19, 2016.....	59
Figure A.24: Magnitude of measured electric field for AUV 7 Run 75 Friday, August 19, 2016.....	59

Chapter 1: Introduction

1.1 Project Overview

The US Navy has shown interest in having the ability to make various types of underwater oceanic survey measurements. These measurements cover a wide range of interests, and one specific area of interest was the measurement of electric and magnetic fields in the ocean. The Office of Naval Research (ONR) has partnered with the University of Idaho (UI) to further the research being conducted on this subject. This research has gone towards improving the Navy's ability to perform magnetic and electric field surveys.

Magnetic and electric field measurements have been used for many purposes in oceanic environments. The oil industry has been one of the largest fields where this research has been applied. Magnetic survey measurements have been used to explore the ocean for petroleum [1]. There was interest in the ability to measure electric fields in the ocean, and that was where this research was focused [2].

The Navy was particularly interested in having a standalone system that could be moved from one autonomous vehicle to another without much hassle. This flexibility would make it easier to measure electric fields in many different environments or situations in which different vehicles were required. Creating an accurate sensor system that could be adapted to different AUVs would lead to more efficient testing and the development of more accurate measurement capabilities for the Navy.

The UI has been developing post-processing analyses to accurately display what was being measured, and whether or not it was in line with the theoretical models that describe the measured fields. To conduct this research, UI researchers used Autonomous Underwater Vehicles (AUVs) equipped with sensors to record measurements of interest. The AUVs were

used to measure either magnetic or electric fields, both of which were important to the Navy. Testing was conducted in a couple different environments including tests at UI as well as at the Acoustic Research Division (ARD) in Bayview, Idaho. Yearly tests and evaluations were also performed at the South Florida Ocean Measurement Center (SFOMC) in Fort Lauderdale, Florida. These tests were vital to the progress and evaluation of this research.

The research in this thesis was focused on the development of the electric field sensors and the analysis of electric field measurements performed with them. Having the ability to analyze the performance of these sensors was vital to determine how to continually move forward with improved hardware and processes. The analysis conducted in this research was used to evaluate the accuracy of the electric field sensors and determine possible paths that could lead to improved measurements. By developing an analysis process of the sensor measurements, this work has revealed new paths to investigate for future progress.

1.2 Current State of the Project

UI has been developing a standalone sensor system for both magnetic and electric field measurements [2, 3]. It was important to quantify the accuracy of the measurements, and to be able to identify where any uncertainty in measurements could stem from. Evaluating these measurements and comparing them to the predicted models were the important topics that were evaluated at this stage of the research.

The standalone sensor package will include the electric field sensor, a magnetometer, the data acquisition system, and the batteries to power the system. This will allow the system to be separate from individual AUVs which will make it useful for multiple vehicles. This system will have the ability to measure both electric and magnetic fields using separate sensors. The electric field probe was attached to the front of the system while the magnetometer was inside

the system housing. The final iterations and design work were being performed at the time of this writing.

It was vital to have the ability to analyze the measured fields and compare them to known models. The measurements were compared to models that will be discussed in this paper. These comparisons were key to evaluating the accuracy of our sensor system and determining what could be done to improve the system. By evaluating these measurements, we could identify where future improvements in the AUV, sensors, and testing process could be made. This paper will discuss the results of these tests and discuss these comparisons.

Chapter 2: Methods

2.1 Testing Strategy and Overview

The main strategy for our testing and research was to use multiple testing environments to evaluate the performance of our electric field sensors and AUV systems. We have a laboratory set up with multiple tanks to take tests on our electric sensors after they were initially fabricated. We also performed regular tests at the Acoustic Research Division (ARD) in Bayview, Idaho. These tests were performed to test the maneuverability of our AUVs with the sensors attached as well as to test our different mission paths. All of these initial tests were performed to prepare for testing at the South Florida Ocean Measurement Center (SFOMC) in Fort Lauderdale, Florida. This was where the most ideal testing occurred. A known source was placed on a moving surface vessel while the AUV operated underneath this vehicle. The main results of this research are from these tests.

2.2 Sensors

Measurements were conducted using silver-silver chloride (Ag/AgCl) electrodes to determine the electric potential in the test environment. These electrodes were used to create custom underwater electric potential (UEP) sensors. We used two sizes of electrodes. The first size was a 2mm diameter cylinder with a length of 4mm. The newest electrodes used were disk shaped and had a diameter of 12mm and a thickness of 1mm.

Three pairs of electrodes were placed in a 7.2cm (3in) diameter spherical mold approximately 7cm apart along with a preamplifier that was then filled with a urethane elastomer compound. This compound was used for its ability to be used in seawater. Two parts, the resin and hardener, were mixed and then poured into the mold. This would then sit for 24 hours to harden. The sensor was attached to a 8cm fiberglass rod that would position the sensor

slightly below and in front of the AUVs [2]. Figure 2.1 shows a representation of the sensor with the embedded electrodes and preamplifier.

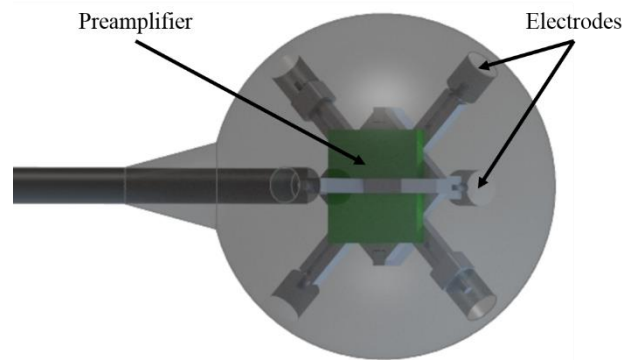


Figure 2.1: 3 inch sensor with embedded electrodes and preamplifier

Three Texas Instruments INA129 preamplifiers were used (one per electrode pair). This was used to provide gains of 250 – 1000 with low noise. More detailed information can be found in [4]. A gain of 250 was used and this amplifier was embedded in the probe as shown above.

The initial design of the electric field sensor was a 3.81cm (1.5in) diameter probe that would then be connected to the preamplifier through the fiberglass shaft. This meant there was approximately 100cm (~ 40in) length of wires running from the sensor through the fiberglass rod to the data acquisition system on the AUV where the preamplifier was located. After initial lab testing and the first test in Florida, we hypothesized that the extra length of wires running along the AUV could be acting similarly to antennas by amplifying noise from the AUV electronics before the measurement reached the preamplifier which was housed in an external can along the AUV.

A new, larger diameter mold was created that could house both the electrodes as well as the preamplifier as seen above in Figure 2.1. This allowed us to connect the preamplifier to the

electrodes without extra wires running through the fiberglass rod along the AUV. By removing this extra length of wires, improvements in our measurements were made which will be discussed in chapter 3.

2.3 Dealing with Electrode Drift in Post Processing

Ag/AgCl electrodes can be used for many marine measurement applications and have been used largely in the petroleum industry [5]. They generally measure small electric signals well with relatively low noise levels. The electrodes measure the electric potential between a pair in volts. To get the electric field E from this, the raw data in volts v was divided by the gain ($g = 250$) of the preamplifier multiplied by the diameter d of the probe as well as a shape factor ($s = 1.5$). Equation 2.1 shows this calculation

$$E = \frac{v}{gds}. \quad (2.1)$$

There were some issues that resulted from the specific application of our use of these electrodes. The biggest obstacle was dealing with potential offset and drift from the electrodes. Drift was the amount of change from where the initial offset of the electrode measurement started the run. Both of these could be reduced by allowing the electrodes to soak in the testing environment for a sufficient amount of time. In other applications, when an electrode pair was placed on the seafloor (stationary) and left there for a long time, the sensor settles to an equilibrium. In some cases, we were able to obtain a sample of the water we would be testing in to allow the sensors to settle before testing. If the sensors were allowed to soak in the same water that they were being tested in, the drift was much less of a factor in the analysis of the measurements. Because our AUVs were constantly in and out of the water, drift had to be analyzed after testing.

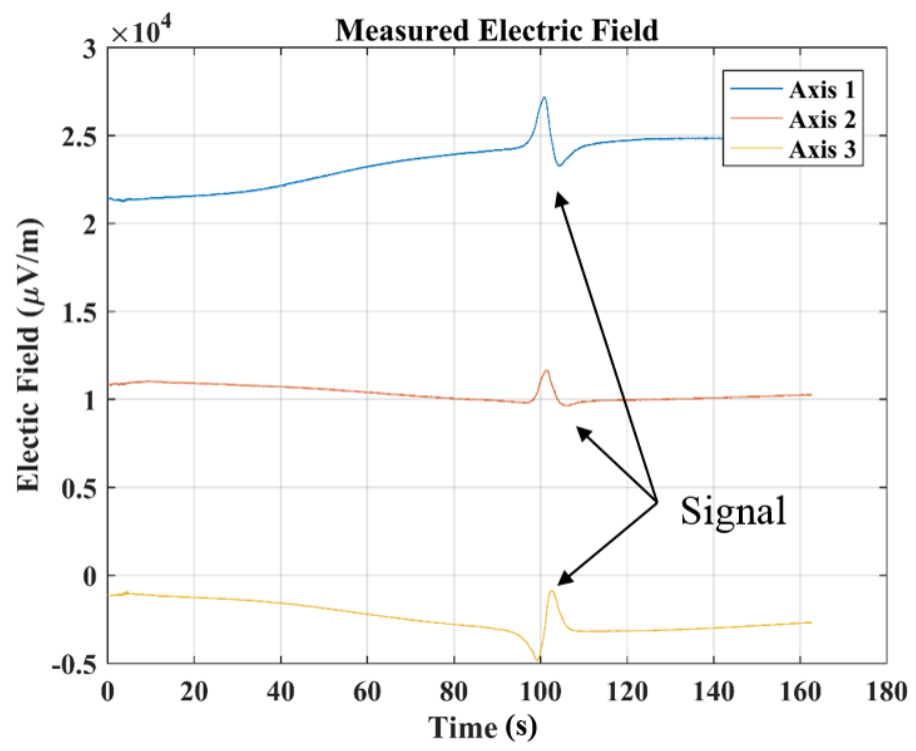


Figure 2.2: Measured electric field from Sub 7 Run 38 from Florida on August 17, 2016

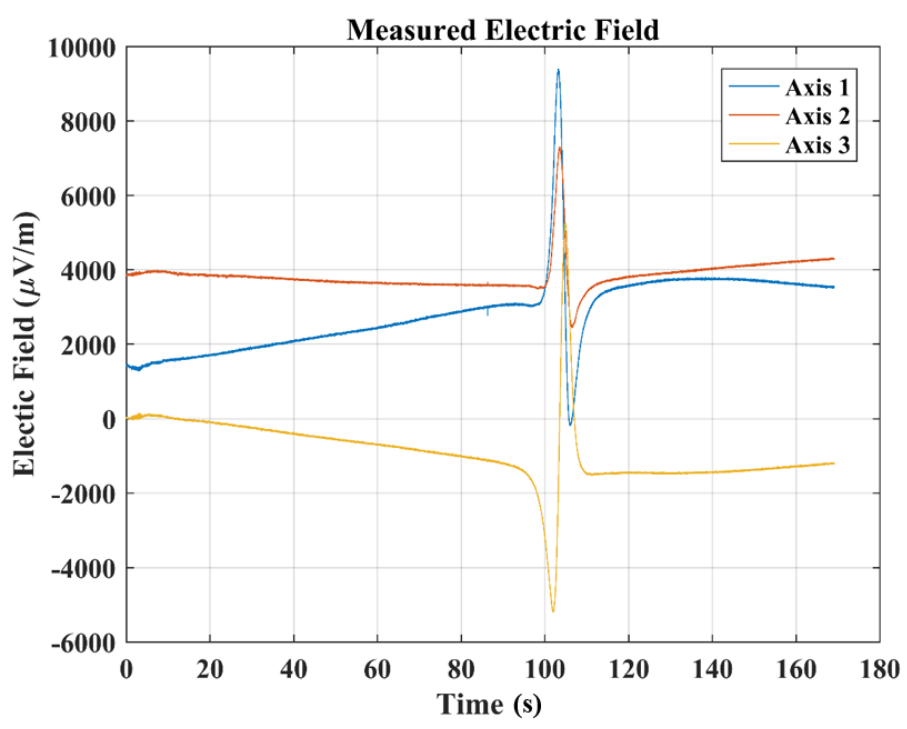


Figure 2.3: Measured electric field from Sub 7 Run 12 from Florida on August 19, 2016

Figure 2.2 and Figure 2.3 show two different runs taken at SFOMC in which the drift and offset were quite different. A controlled DC signal on a moving source boat was measured. Each line on the plot was the measured electric field of a pair of electrodes. Figure 2.2 was a run from Wednesday August 17, 2016. The sensor did not get to soak in the water that we tested in. This lack of soaking lead to a much higher offset, slightly more than 20,000 micro volts per meter ($\mu\text{V}/\text{m}$) for one electrode pair, than in Figure 2.3, roughly 1,500 $\mu\text{V}/\text{m}$. The sensor soaked for over 40 hours before the test in Figure 2.3 which was why the offset was so much lower.

The drift was also affected by how long the sensor was allowed to soak and get close to equilibrium. The largest difference between the start and end of the run in Figure 2.3 was roughly 2,000 $\mu\text{V}/\text{m}$ compared to 3,500 $\mu\text{V}/\text{m}$ on Wednesday. Because the drift varies between runs, it was important for us to be able to remove the drift to better analyze the output signal from the source.

Figure 2.4 and Figure 2.5 show what the measurements looked like after the fit of the trend and the offset were removed. The first step shown in Figure 2.4 was to remove the output signal, the signal that was placed into the water, from the remainder of the electric field. Because our runs were all set up along the same path, the duration of the output signal in time was approximately the same for each run, roughly 30 seconds. This section was removed and the remaining measurement was fit with a cubic polynomial as shown in Figure 2.4. The polynomial was then subtracted from the original measurement of the electric field to obtain the results shown in Figure 2.5. This was the measurement that was then used to calculate the magnitude of the electric field which will be discussed in the following section. The thick lines in the figure show the original electric field with the signal removed while the

black lines in the middle of each represent the polynomial that was subtracted from each channel.

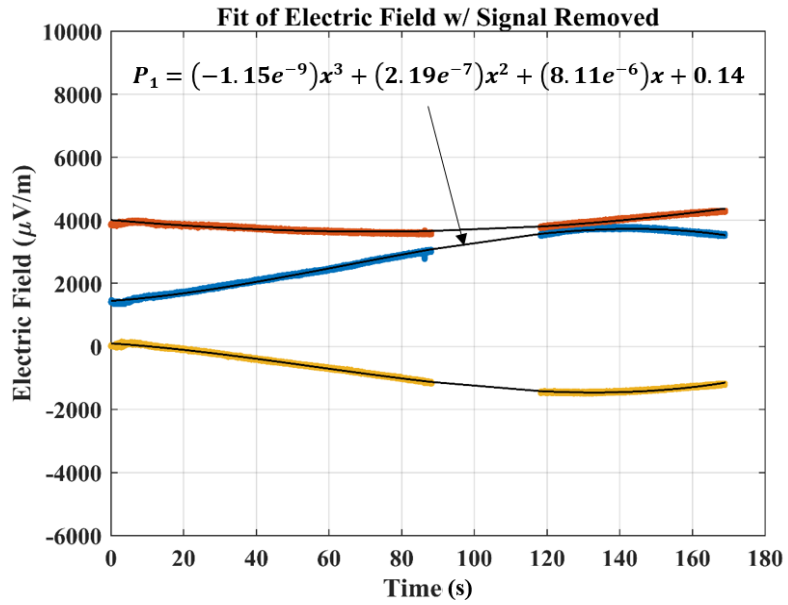


Figure 2.4: Electric field measurement with a cubic polynomial fit

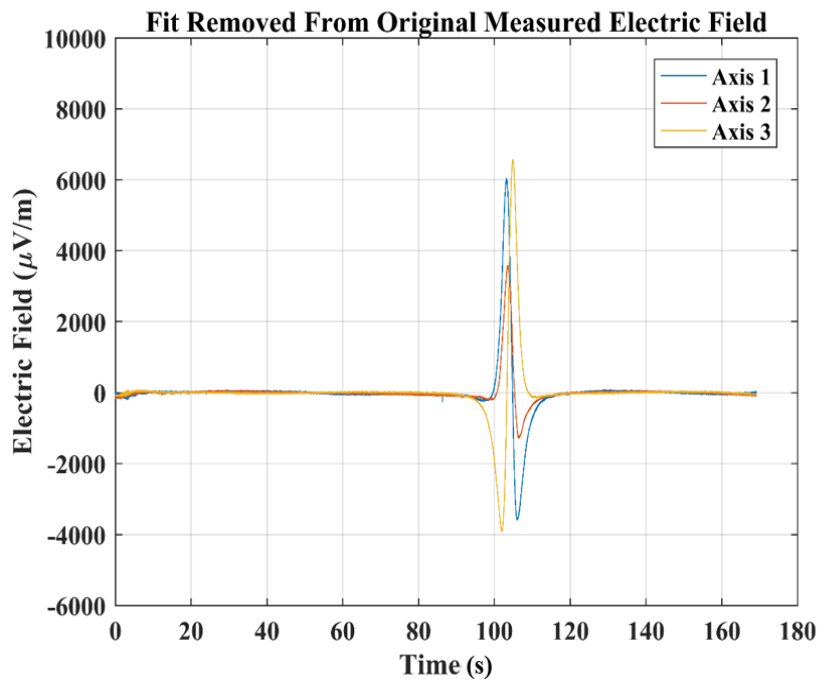


Figure 2.5: Electric field measurement after the polynomial fit is removed

2.4 Electric Field Modeling

By comparing our measurements of the electric field to theoretical models, we could examine how accurate our measurements were to what was physically happening. The model consists of three layers: air, seawater, and the seafloor [6]. The source q was located in the seawater and the observation point P represents our AUV. Everything $z > 0$, comprised the air while $-d < z < 0$ comprised the seawater, and $z < -d$ represents the seafloor. Figure 2.6 shows a representation of what was expected from the images, or reflections, of each boundary. The images were represented by $c_n, d_n, c_0, d_0, a_0, b_0, a_n,$ and b_n .

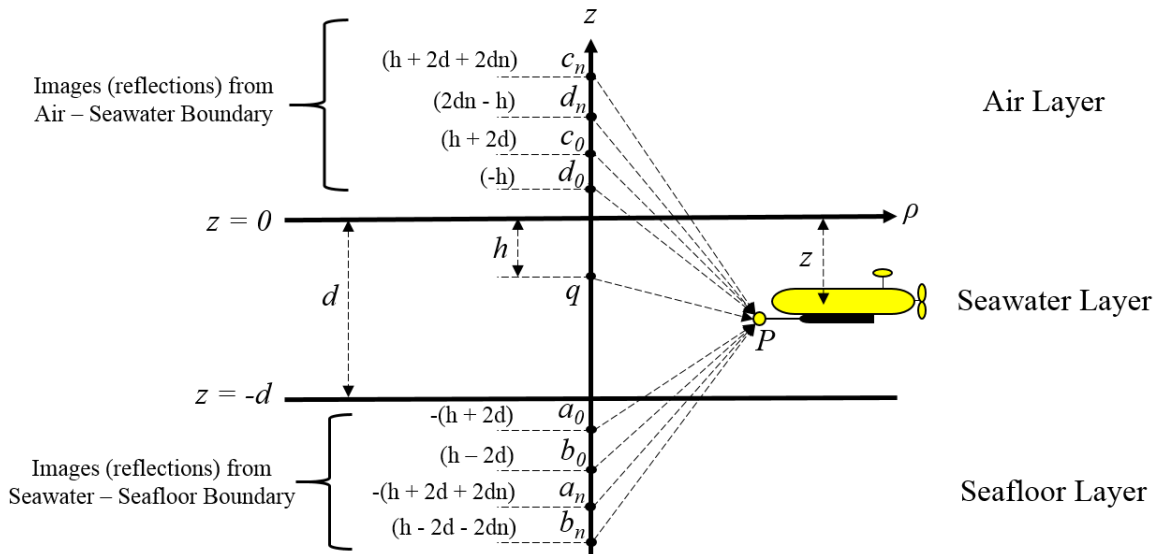


Figure 2.6: A representation of reflections from boundary effects

The following equations from [6] were used to evaluate our experiments and determine the effects of both the free space and layers:

$$V = \frac{K_2}{r} + K_2 \sum_{n=0}^{\infty} \left[R_{23}^n R_{21}^n \left(\frac{R_{23}}{r_a} + \frac{R_{23} R_{21}}{r_b} + \frac{R_{23} R_{21}}{r_c} + \frac{R_{21}}{r_d} \right) \right], \quad (2.2)$$

$$K_2 = \frac{j\omega q}{4\pi Y_2}, \quad (2.3)$$

$$Y_i = \sigma_i + j\omega\epsilon_i, \quad (2.4)$$

$$E = -\nabla V. \quad (2.5)$$

Equation 2.5 was used for the total field calculation. This was the model used to determine both the free space and the layered effects of our test conditions. The first part of (2.2) before the summation, accounted for the free space field of the source. The summation term of the model incorporated the effects of the images reflection from the boundaries. The value for ω was close to zero (0.00001) to be used for dc measurements.

The boundaries were broken down into three layers. The first layer, or $i = 1$, was air. The second layer was the sea water the AUVs operated in, and the third layer was the sea floor. The admittance between boundaries (2.4) was based on the conductivity, σ , and permittivity, ϵ , of the layer. The remaining components of (2.2) dealt with the reflection effects of the boundaries and the locations of those reflections as shown in the following equations [6]:

$$R_{21} = \frac{Y_2 - Y_1}{Y_2 + Y_1}, R_{23} = \frac{Y_2 - Y_3}{Y_2 + Y_3}, \quad (2.6)$$

$$r_a = \sqrt{\rho^2 + (z + h + 2d(n + 1))^2}, \quad (2.7)$$

$$r_b = \sqrt{\rho^2 + (z - h + 2d(n + 1))^2}, \quad (2.8)$$

$$r_c = \sqrt{\rho^2 + (h - z + 2d(n + 1))^2}, \quad (2.9)$$

$$r_d = \sqrt{\rho^2 + (2nd - z - h)^2}. \quad (2.10)$$

These equations take into account the characteristics of the position of the source as well as the properties of each layer. The distance from the measurement point P (sensor on the AUV) to image a , was given by (2.7). The remaining equations (2.8, 2.9, and 2.10) were the distance from the image to the AUV. The coordinate ρ , the horizontal distance of the AUV to the source,

and z account for the position of the AUV in the water, and n was the number of images or reflections. The depth of the source in the water was given by h , and the depth of the water was given by d . For the tests performed at Florida in August, 2016, the depth of water d we tested in was on average 30 meters.

The properties of each layer were important to increase the accuracy of the model. The values of these properties, the conductivity and relative permittivity of each layer, were used based on given ranges from literature. The conductivity of air used was $\sigma_1 = 5.5e-15$ Siemens per meter (S/m). This value was taken from [7], where a range of values for the conductivity of air was evaluated over the Indian ocean. The conductivity of seawater, $\sigma_2 = 4.8$ (S/m), was taken from [8], and the conductivity of the seafloor, approximately $\sigma_3 = 5$ (S/m), was found from [9]. Conductivity, the inverse of resistivity, was given in [9]. This value was then used to calculate the conductivity of the seafloor that was used in the model.

The permittivity was calculated by finding the relative permittivity of the seawater and seafloor layers, and then multiplying that value by the permittivity of free space, $\epsilon_1 = 8.85e-12$ Farads per meter (F/m). The relative permittivity of seawater, $\epsilon_{r2} = 70$, was found in [10], and the relative permittivity of silt, $\epsilon_{r3} = 30$, was found in [11]. These values were taken from inside of given ranges for these properties. Changing these properties, both the conductivity and permittivity, varied the results of the model slightly. There were other factors which impacted accuracy of the models much more significantly, mainly the accuracy of the position of the AUV.

We used these models to create iso-electric field surface plots to examine the electric field created by the source from our second set of field tests from Florida. During ocean testing, the source boat used two electrodes in the water which created a dipole. Figure 2.7 shows three

stages of the model using these plots to visualize the electric field that was created by the source.

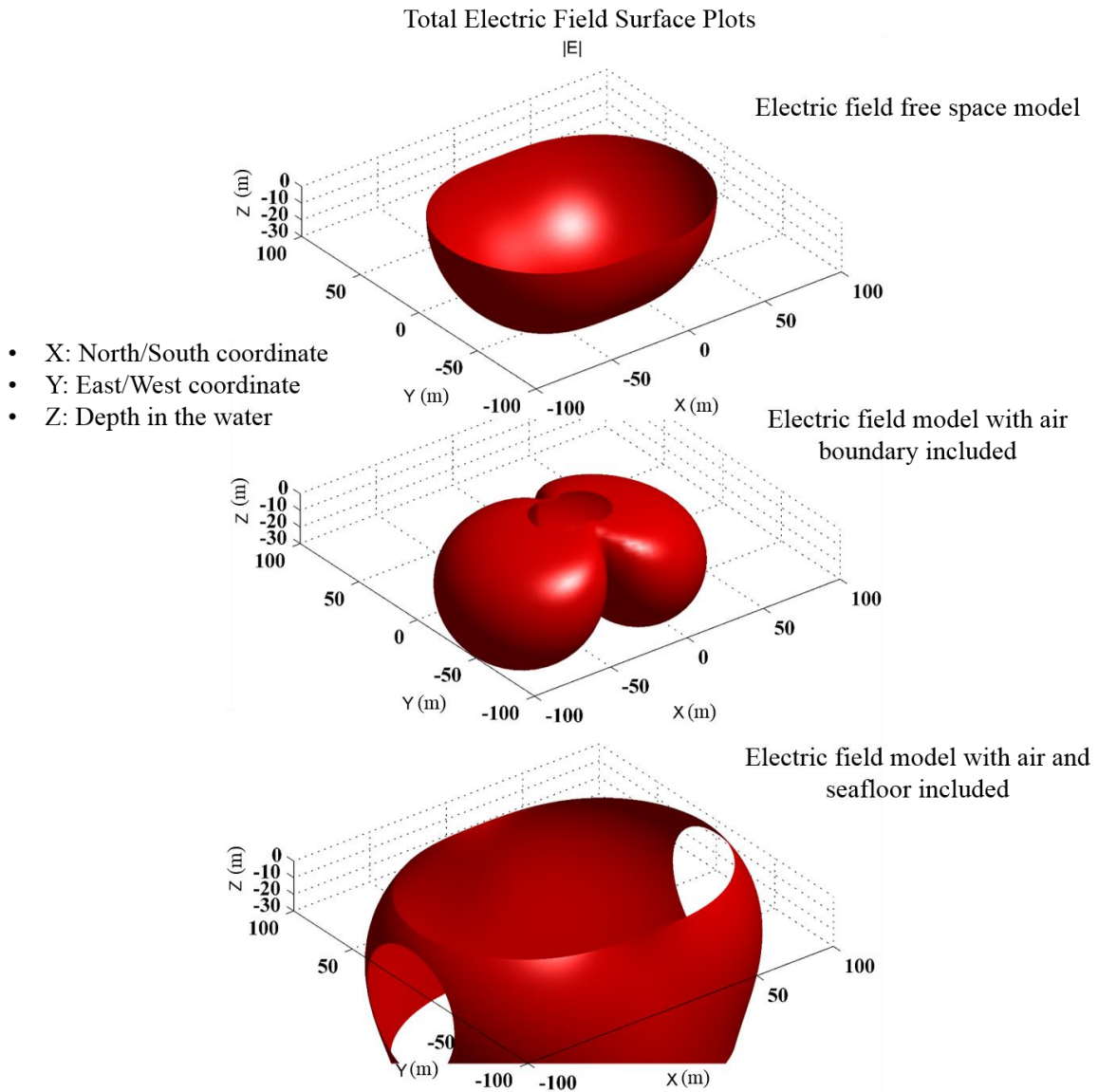


Figure 2.7: Visualization of electric field created by source boat during Florida ocean tests

The surfaces of constant electric field magnitude used for these surface plots were 10^{-6} $\mu\text{V}/\text{m}$. The first image shows the electric field of the dipole source in free space with no boundaries. The second image adds the effects of the top layer (air), and the third image adds the effects of the bottom layer (seafloor) as well. This shows that the air layer reflections seem

to stretch the field in the x coordinate which allows us to see the dipole more clearly. By adding in the effects of the seafloor, the entire field was stretched vertically in the z direction. The intermediate steps between these images were not shown here, but it was important to note that the intermediate steps were continuous between the images.

2.5 Noise Floor Measurements in the Lab

We examined the amplitude spectral density of measured electric fields in a controlled environment with the ambient field minimized to determine whether or not our electric field sensor was meeting the given noise requirements. This requirement was that the RMS noise needed to be approximately in the 0 – 10 Hz bandwidth when measuring background noise in a quiet lab environment.

2.6 Lab Testing Apparatus and Process

Much of our initial testing was performed in a lab setting at the University of Idaho. Most of the testing conducted in this setting was to determine if the sensors were fabricated correctly. The goal of these tests was to examine the noise floor and response to controlled signals in the test environment.

Figure 2.8 shows a standard set up for these experiments. The AUV was strapped to the mounting rack as shown and was set up to record based on what mission was sent to the AUV. The data acquisition system was set to read samples at 16.6 kHz at 16 bit resolution. We had a mission set to solely record data and run everything on the AUV but the motor until the mission was aborted and we could retrieve the data for analysis. The AUV, with sensor attached, was placed in a 125 gallon tank, roughly 4' by 3', with salt water prepared to approximately the same salinity levels as were measured off the coast of South Florida. This was done to replicate the expected testing environment as closely as possible. As shown in the following figure, the

stainless steel plates, approximately 3” by 5”, were placed in the tank on each side of the sensor roughly 2’ apart. The plates had leads coming off of them to attach a current controlled source which was used to input various different signals into the tank.

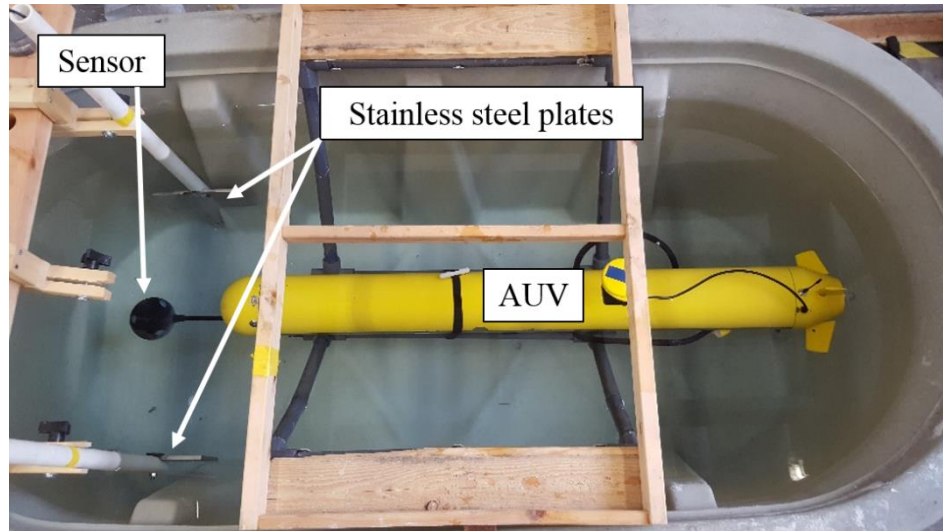


Figure 2.8: Lab set up for testing electric field sensors

It was important to determine the noise floor of our sensor when operating on the AUVs so that we had a reference for what should be expected during testing. The sensors were tested initially without the AUVs, but these tests were used only for evaluating whether or not the probe was manufactured well. Our noise floor measurements were conducted with the AUVs because this would be the normal operating configuration.

A Faraday cage was built to help reduce noise from surrounding labs, buildings, and power sources. The cage was approximately 10’ long by 8’ wide and 8’ tall. The frame was built using wood, and the mesh was a fine aluminum mesh attached to the outside of the frame as shown in the following figure. The floor was not covered during these tests. The sensors were tested in this environment to mirror what would be expected in an ocean setting.



Figure 2.9: Faraday cage in lab

2.6.1 - Response to a Controlled Electric Field Source

Testing our sensors to see how well they measured controlled signals in our lab environment was key to evaluating whether or not they were manufactured correctly, and if they were ready to be used in the field. The electric field sensors were attached to an AUV and placed in our saltwater tank. Two stainless steel plates were attached to a source which was used to input signals into the water. Different ranges of signals were tested and the measurements were recorded for analysis. This was the final step in evaluating our sensors and their functionality. If a sensor was correctly measuring the given signals, it was then ready to be used in taking field measurements.

2.6.2 - Signal Analysis

A few steps were taken to compute the amplitude spectral density measurements. First, the time series of the measurement was divided into short segments. Each of these segments were then individually de-trended with a straight line fit. The de-trended data was then low pass filtered at 20Hz to remove any larger outside noise. Once these steps were finished, Bartlett's method was used to compute the amplitude spectral density.

2.7 Field Testing

Field tests were performed at the Acoustic Research Division (ARD) in Bayview, Idaho and the South Florida Ocean Measurement Center (SFOMC) in Fort Lauderdale, Florida. These testing facilities were vital in evaluating the progress of our electric field sensors.

2.7.1 - ARD at Bayview

Testing was conducted at ARD in Bayview, Idaho to develop the missions and strategies that would be used for testing in Florida. ARD, located on Lake Pend Oreille, was perfect for testing any upgrades or developments not related to the electric field sensors. In general, most navigation techniques were developed and tested here to prepare for testing in an ocean environment in Florida. It was also important to test our command station and the controls that we used to operate and communicate with the AUVs. This was a great place to evaluate all of the steps and procedures that led to the AUVs performing well during ocean testing.

The range we operated in was roughly 150m by 75m and the depth of the lake was 25m – 50m depending on the time of year. We deployed four buoys in the range and the AUV received four ranges every 2.5 seconds. A top side tracking system was used by the researchers at ARD to track the position of the AUV.

Because Lake Pend Oreille is freshwater, our Ag/AgCl electrodes did not perform well in terms of measuring of background noise or electric fields. This lack of ability to test our electric field sensors in freshwater led to supplementing these tests with lab testing of the electric field sensors to determine their effectiveness.

2.7.2 - Florida: April 2016

In April 2016, we took a weeklong trip down to SFOMC to evaluate our electric field sensors in the ocean. The plan was to spend some time testing off the side of one of the piers

on base, and then to also take the AUVs offshore into a deeper testing range away from possible noise sources. Unfortunately, there was a scheduling issue that prevented us from being able to use the offshore range, so our testing from that week was all conducted pier side. The biggest obstacle this presented was a louder background environment due to other objects in the water such as cruise ships, recreational boats, and other sources that could potentially create noise.

We were able to run many tests off the pier shown in Figure 2.11 to evaluate the noise floor as well as the ability of our sensors to detect electric fields that were placed into the water. The test consisted of a simple pattern that we called a lawnmower mission. The AUV would start the mission at one end of the pier approximately 3m away from the pier which was where the source was placed into the water. The AUV would then run in a straight line for 15m before making a turn away from the pier for a 1.5m and then turn to head back to the beginning of the pier. Two of these patterns would take place during one mission. This allowed the AUV to pass the source multiple times during run. We had other missions as well that varied the length and number of turns the AUV made. This range was roughly 60m by 50m and the depth varied anywhere from 2.5m to 7.5m depending upon the tides.

The electric fields were generated in the water using two copper plates shown in Figure 2.10 that were attached to a signal generator. The signals input were varied to create AC and DC signals. The following two figures show the copper plates that were used as well as a picture of the AUV off the side of the pier.



Figure 2.10: Copper plate used to create desired electric fields



Figure 2.11: AUV off the pier at SFOMC

2.7.3 - Florida: August 2016

The second week of tests performed in Florida during 2016 was focused on offshore testing since only pier side tests were taken during the previous Florida tests. The goal of these tests was to evaluate the magnetic and electric field sensing capabilities of our sensor systems. We wanted to be able to operate our AUVs in an ocean environment with minimal environmental noise to evaluate how well our sensors performed. These tests provided the opportunity to evaluate how our system would perform in an applicable scenario.

We loaded up all of our equipment and AUVs onto a boat and spent roughly 40 minutes heading out to the offshore range where we deployed our AUVs to begin running missions. This range was 200m by 200m and the depth was approximately 16m. There was also a separate source boat (Parker boat) that was used for putting signals into the water. The source boat was roughly 7.6m long and placed 30 Amps of current through electrodes attached approximately 0.4m below the water line.

The objective was to have the AUV run in a straight line at 10 meters of depth while the source boat ran in a straight line in the opposite direction on the surface. By running this sort of mission, we were able to examine how well our sensors could detect the given signal with very little background noise and interference.

These experiments resulted in valuable data that could be analyzed to determine the effectiveness of our system. We obtained both electric and magnetic field runs that would be used to evaluate the performance of our sensors and system as a whole. These measurements and the results of their analysis will be discussed in this paper.

Chapter 3: Results & Discussion

3.1 Measurement and Analysis of Signals

The results discussed in this thesis will focus mainly on the progression from lab testing to field testing of the electric field sensor and the analysis of measurements taken in each phase. Lab testing was focused on evaluating the noise floor of the electric field sensors as well as their capability to measure known signals. Field testing focused on the performance of electric field sensors in ocean environments. The analysis of these measurements was conducted to determine the effectiveness of our sensors, and where improvements could be made in future development.

3.1.1 - Lab Testing of Electric Field Sensors

The first goal of testing the electric field sensors in a lab was to determine their noise floor in a controlled environment. This gave an idea of where the baseline should lie for the sensors. The following two figures show the results of the tests with electric field signals explained in section 2.6 where plates were placed in the test tank to generate a voltage in the water. These figures display the amplitude spectral density for both the 1.5” and 3” probes with no voltage applied to the plates.

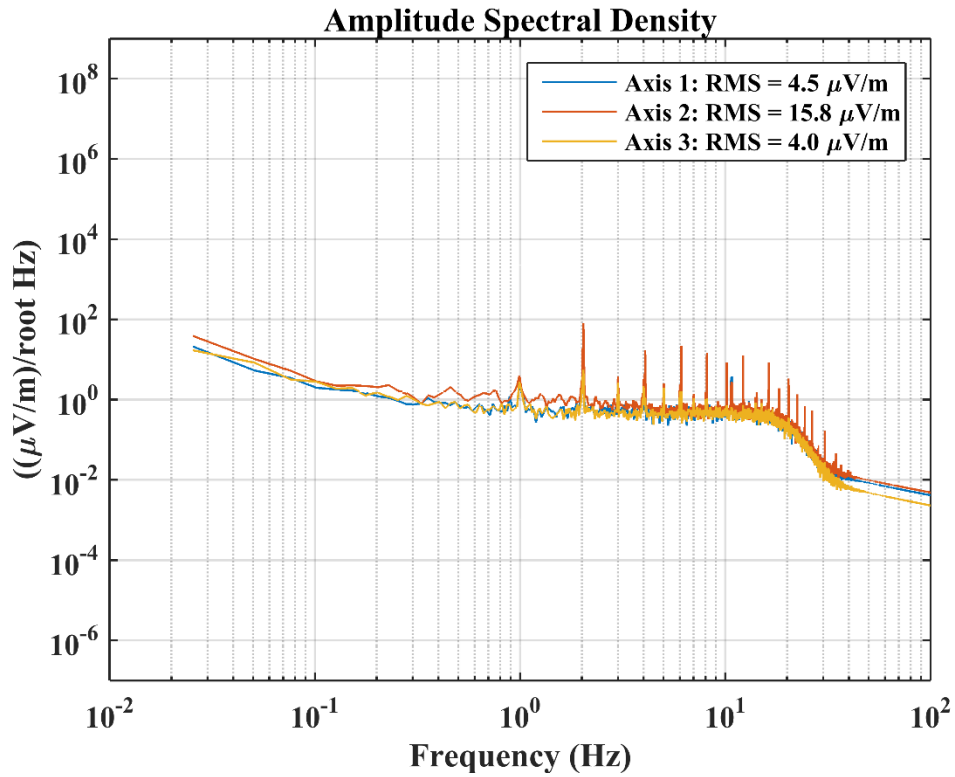


Figure 3.1: Amplitude spectral density of 3.81cm (1.5") diameter probe with cylindrical electrodes (preamp outside probe)

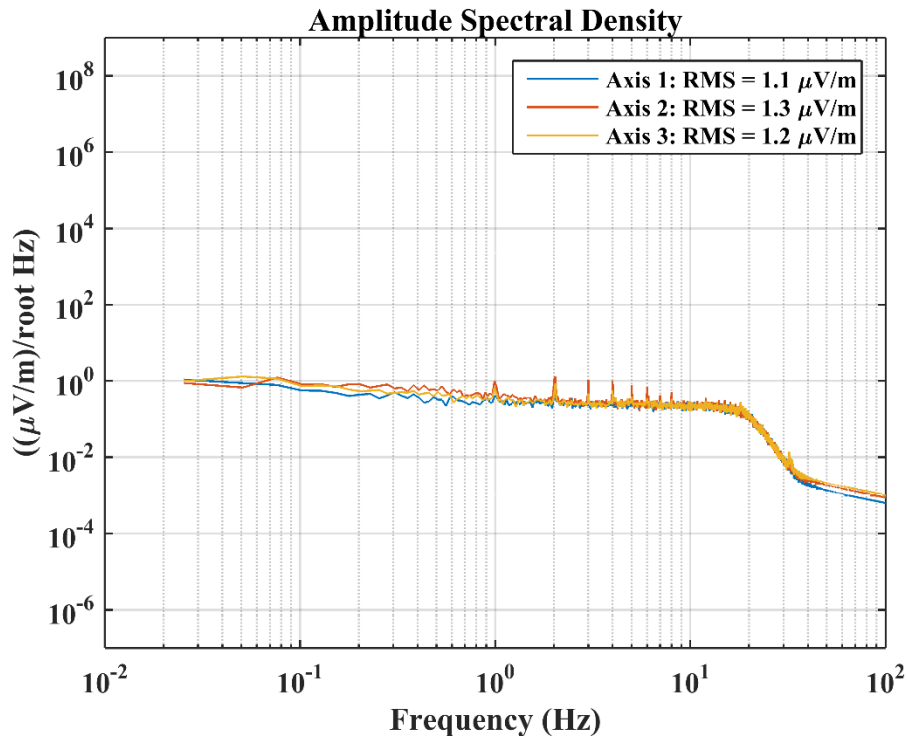


Figure 3.2: Amplitude spectral density of 7.2cm (3") diameter probe with cylindrical electrodes (preamp inside probe)

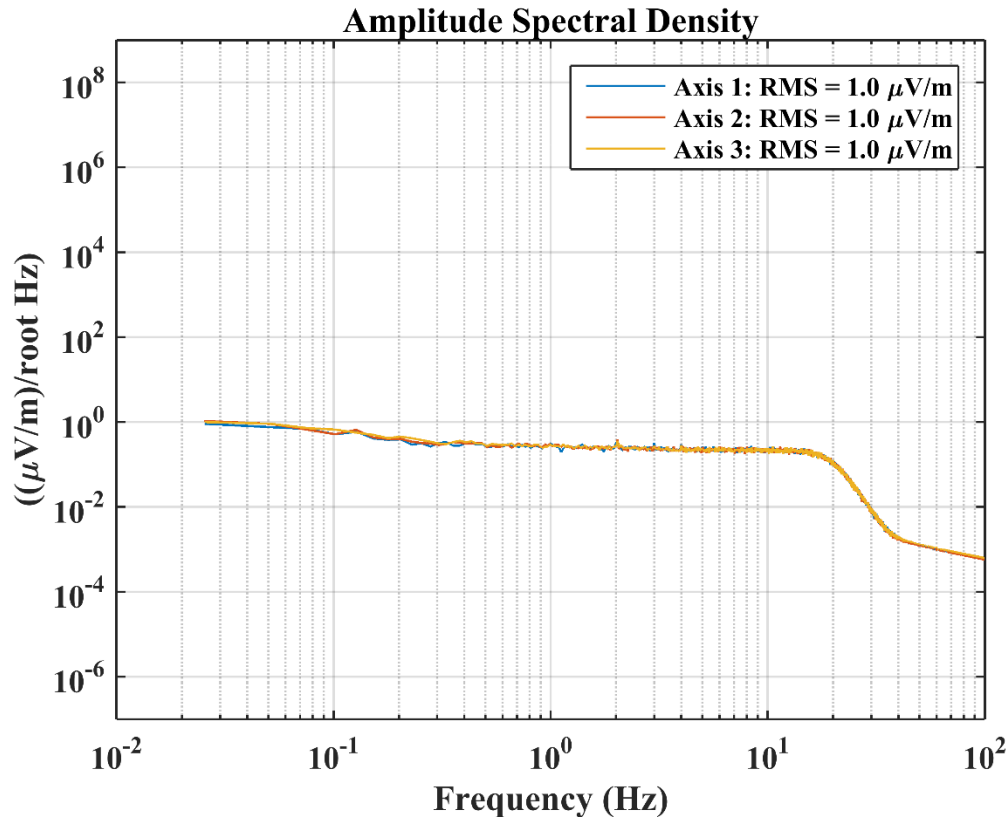


Figure 3.3: Amplitude spectral density of 7.2cm (3") diameter probe with disk electrodes (preamp inside probe)

Figure 3.1 and Figure 3.2 show the reduction in noise from moving the preamplifier inside the probe. For the 1.5" diameter probe in Figure 3.1, the RMS values range from 4 $\mu\text{V}/\text{m}$ to 15.8 $\mu\text{V}/\text{m}$. These values drop significantly for the 3" diameter probe with the preamp inside in Figure 3.2 to low and high values of 1.1 $\mu\text{V}/\text{m}$ and 1.3 $\mu\text{V}/\text{m}$. These RMS values for the probe with the preamplifier inside were much closer to the target value of approximately 1.0 $\mu\text{V}/\text{m}$. Figure 3.3 shows the 3" diameter probe with the disk electrodes replacing the cylindrical electrodes. This brought us down to the goal of 1.0 $\mu\text{V}/\text{m}$ RMS.

The other observation to take from Figure 3.1 and Figure 3.2 was the integer noise spikes at 1, 2, 3, 4 Hz etc. A signal appeared to be picked up from some component of the AUV. It can be seen that the spikes were much larger in the 1.5" sensor than in the 3" sensor where the

preamplifier was embedded in the probe with the electrodes. This helped provide evidence for the theory that the long length of wires that ran from the electrodes to the preamplifier in the first sensor were amplifying noise sources from the AUV. With the preamplifier embedded inside the probe, much of this noise was reduced. The source of this signal was not identified, but further investigation into the cause was being conducted. It is important to note that because of the relatively quiet test environment of the lab, this signal was noticeable whereas in field testing, this noise source would not be seen.

The second purpose for testing in the lab was to verify that the sensors could measure electric signals placed in the test tanks. If the sensors could measure the known signal, this would be a good indication that the sensors were ready for field testing. The following figure shows what the amplitude spectral density would look like for these tests.

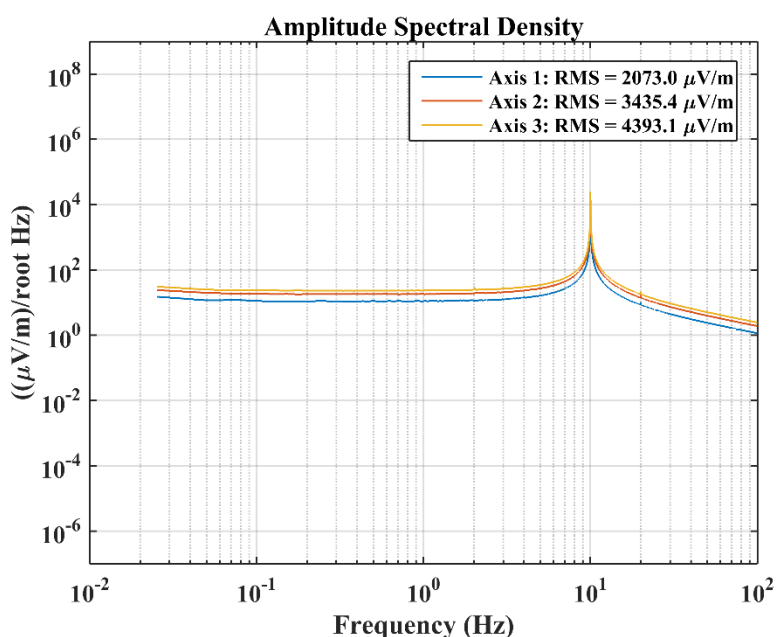


Figure 3.4: Amplitude spectral density for a tank test with a 10 Hz signal in the water

Figure 3.4 shows the outcome of these tests when the sensor is fully functional. The 10 Hz signal at 0.1 Amps was very strong and the sensor was able to measure it well. If something

similar to this was not the result of testing a sensor, it was helpful to troubleshoot if there was a manufacturing error with the probe. We tested various signal levels, and the results all looked similar to this plot with spikes matching the source signal frequency.

3.1.2 - Tests Taken Along Pier at SFOMC

Pier side testing was conducted from April 4th, 2016 through April 8th, 2016 in Florida at the SFOMC. These tests were conducted to obtain measurements of electric fields from various types of signals to evaluate the performance of our electric field sensors. The 3” diameter electric field probes were not constructed until after this set of tests, so the 1.5” diameter electric field probe with cylindrical electrodes was used. Figure 3.5 and Figure 3.6 show the background measurements of the ambient electric field of the environment before electric signals were introduced. This was used to give a baseline of performance for the electric field measurements.

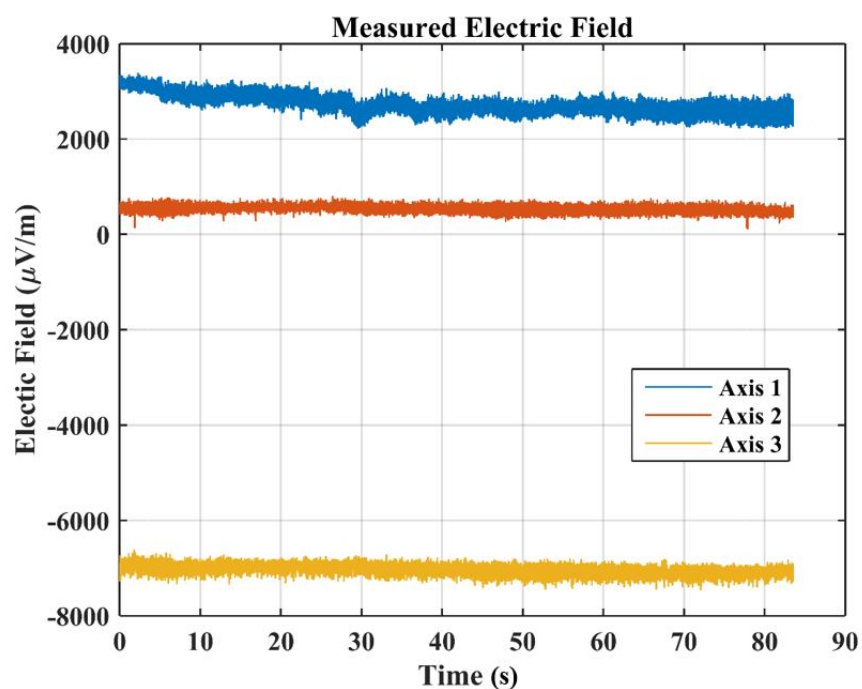


Figure 3.5: Electric field measurement of ambient field pier side

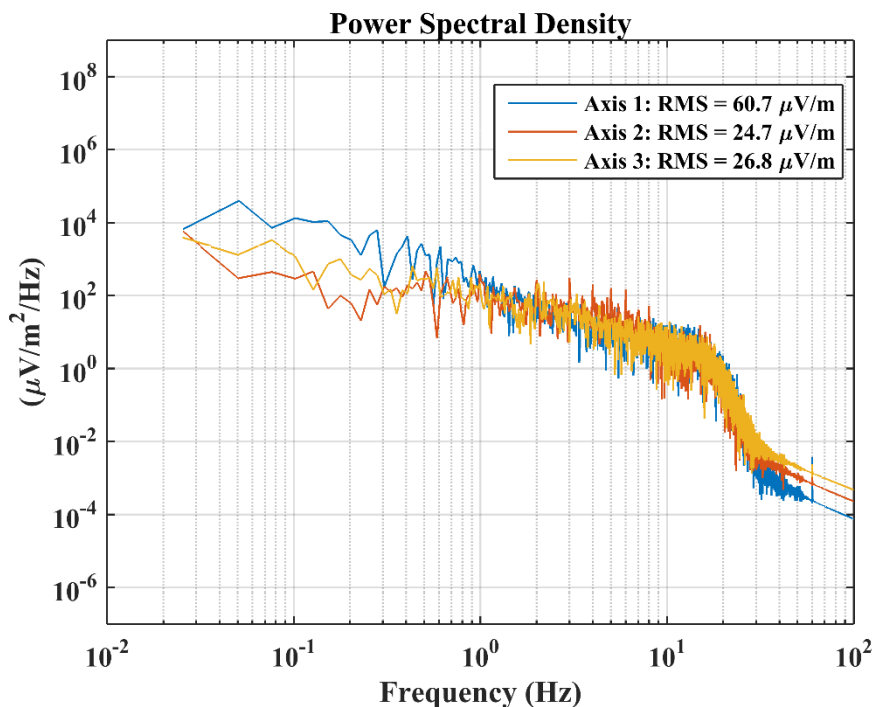


Figure 3.6: Amplitude spectral density of ambient field measurement pier side

Figure 3.5 shows the measured electric field of a run when the AUV was moving three meters parallel to the pier at roughly 3m depth for 40m. This gives a good view of the ambient electric field of the testing environment. There was some offset of the electric field on the electrodes which was normal, and there was very little drift on each pair. The largest amount of offset was on the 3rd axis which was approximately 7,000 $\mu\text{V}/\text{m}$. The drift was also really small where the largest amount of drift was on the 1st axis and was approximately 500 $\mu\text{V}/\text{m}$ over 80 seconds. This was because the electrodes had spent enough time in the environment to come close to stabilizing.

The next plot, Figure 3.6, was the amplitude spectral density evaluation of the electric field time series. This was a good comparison to the noise floor measurements taken in a lab setting at UI shown in Figure 3.1. The RMS values of each pair of electrodes for this measurement ranged from 24.7 $\mu\text{V}/\text{m}$ to 60.7 $\mu\text{V}/\text{m}$. Comparing these values to Figure 3.1, we see that the

overall noise level was higher, approximately a couple orders of magnitude, in the pier side environment than in the lab shown in Figure 3.1. This was expected as there were more sources for ambient noise around the pier than in the lab. It is also worth noting that the 2 Hz signal we saw in the measurement in the lab was buried under the ambient noise in these measurements. We believe it was probably still there, but that it was much smaller than the surrounding field.

The next two figures show the electric field measurements and amplitude spectral density plots for two different runs. The first pair of figures show measurements from a test where a 1 Hz sine wave voltage at 2 Amps was applied to the plates in the water discussed in section 2.6. The second pair shows the same test, but with a 10 Hz sine wave. These represent the capability of our sensors to measure known electric signals in the ocean.

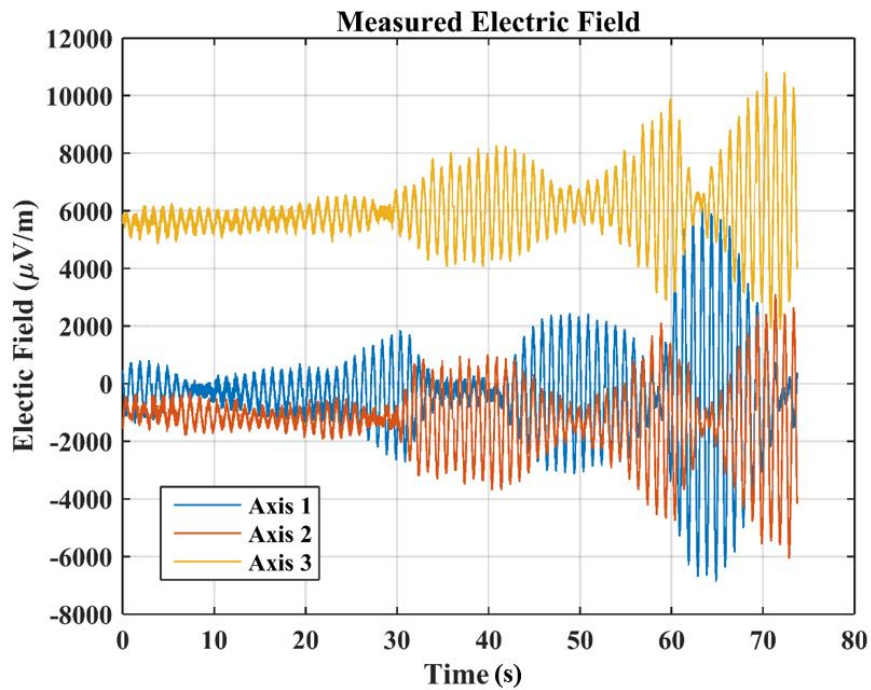


Figure 3.7: Electric field measurement of 1 Hz source signal pier side

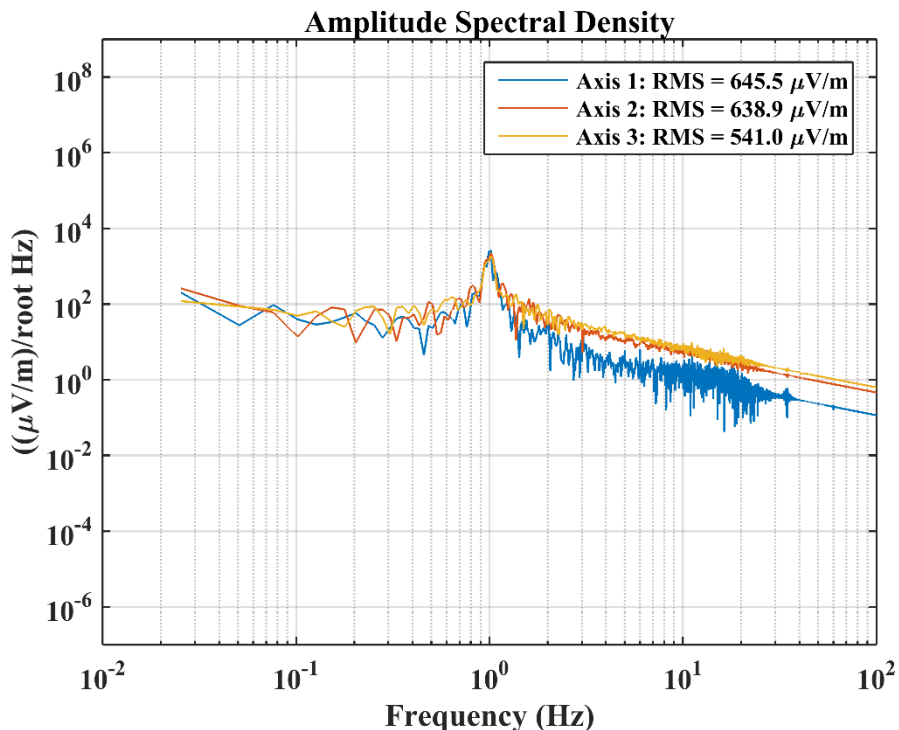


Figure 3.8: Amplitude spectral density of 1 Hz source signal pier side

The 1 Hz input signal can clearly be seen in the electric field plot in Figure 3.7 and the amplitude spectral density plot in Figure 3.8. Looking at the electric field plot the nature of the signal being a sine wave was very clear. The frequency was low enough, even at this scale, that each wave could clearly be seen. The amplitude spectral density plot in the second figure shows clearly the 1 Hz signal from the source. The spike at 1 Hz was very clear and much stronger, by a factor of at least 10, than the ambient noise in the environment.

The next two plots, Figure 3.9 and Figure 3.10, show the same set up with a 10 Hz sine wave at 2 amps in the water. The sine wave was not as easily seen in the electric field time series plot because the frequency was 10 times as high. Zooming into this plot shows the 10 Hz sine wave as clearly as the first test. The spike at 10 Hz in the amplitude spectral density plot was also very clear. These figures made it easy to see how our sensors were clearly measuring the known artificial signals that were being placed into the water.

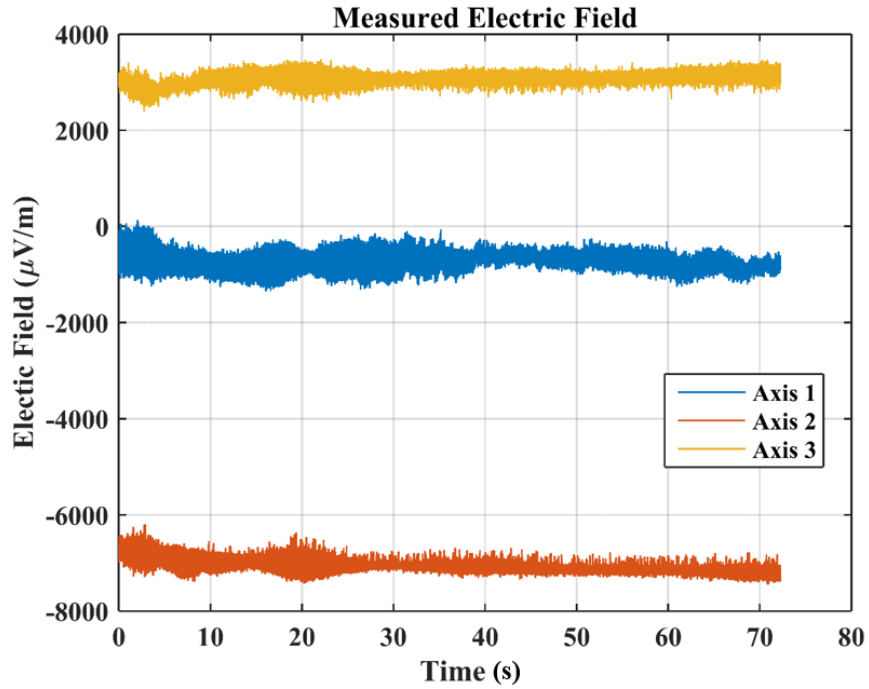


Figure 3.9: Electric field measurement of 10 Hz source signal pier side

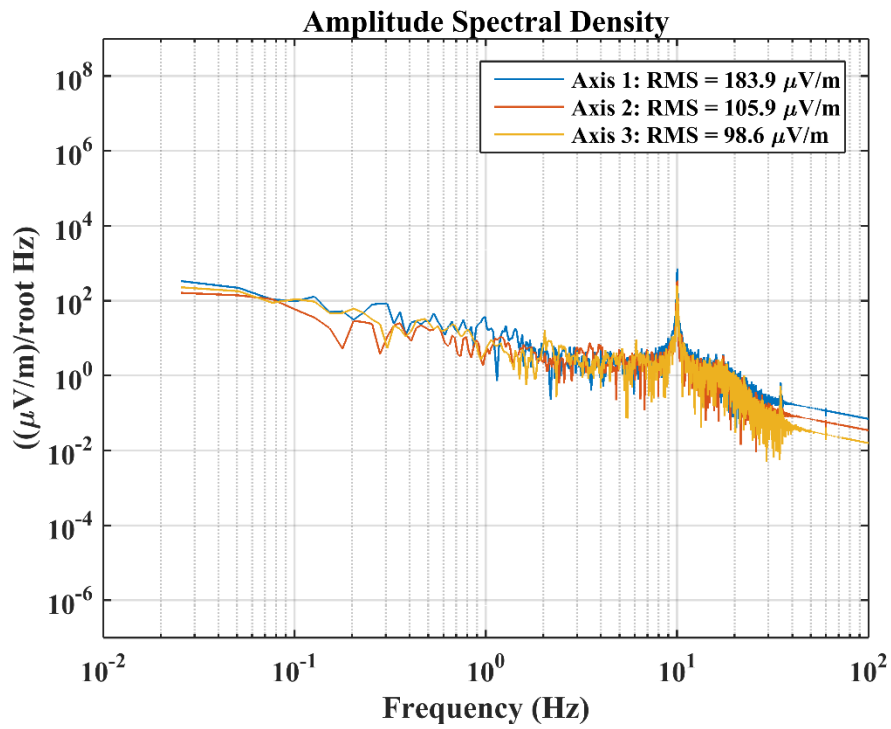


Figure 3.10: Amplitude spectral density of 10 Hz source signal pier side

It was also important that much lower frequency ranges could be measured. To begin evaluating this, we placed a DC signal in the water and continued to run the AUV by the source to examine what was being measured. The source voltage ranged from 0.5V to 10V and the current ranged from 1A to 10A. These next figures show the measurements of the DC electric field signal in the water. Four amps were applied to the plates for this measurement.

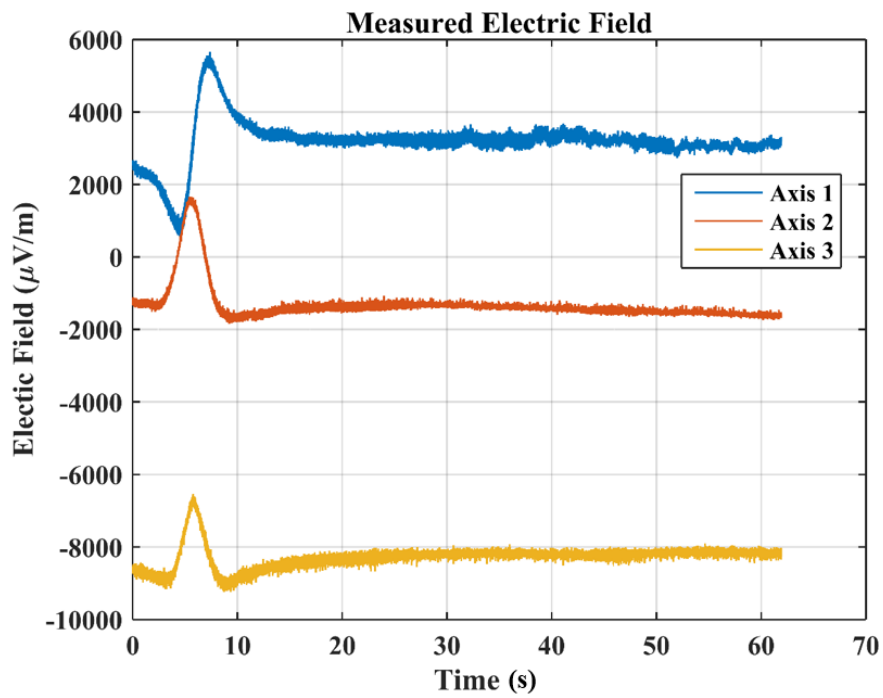


Figure 3.11: Electric field measurement of DC signal pier side

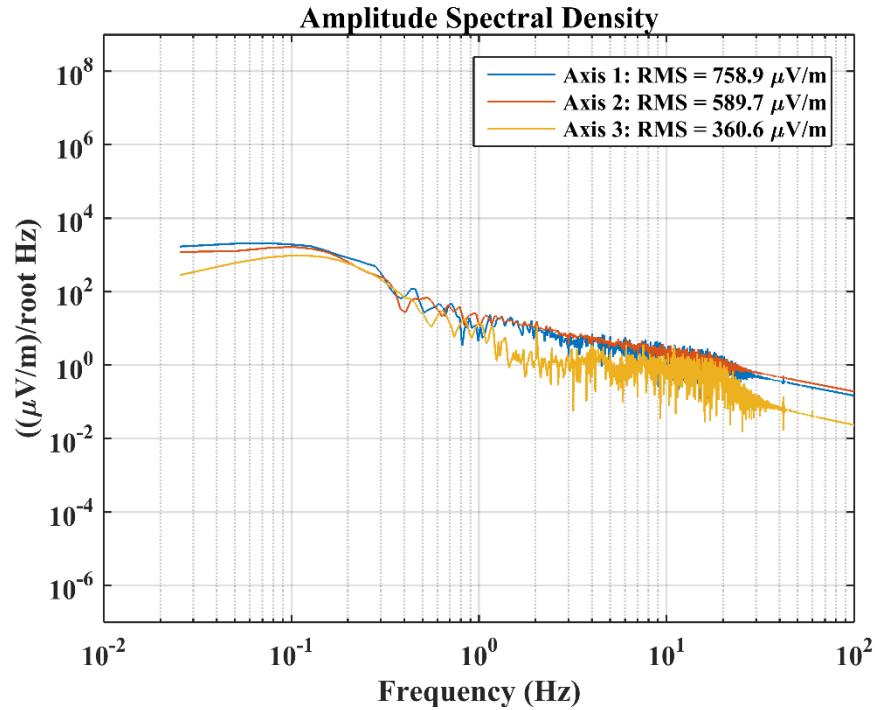


Figure 3.12: Amplitude spectral density of DC signal pier side

A couple important pieces of information can be gained from these plots. Examining Figure 3.11, the position of the source can be seen. The AUV was running alongside the pier where the source was mounted, and the AUV passed the source at the beginning of the run. This can be seen in the first 10 seconds of the plot and agrees with the physical set up of the run. This would be similar to what could be seen if the AUV was driving next to an object in the water that was giving off a low frequency electric signal. Figure 3.12 shows the amplitude spectral density plot from this run. The low frequency noise in this plot, 0.01Hz to 0.2Hz, was approximately an order of magnitude, around $10^3 \mu\text{V}/\text{m}$, higher than the tests involving no signal or a sine wave input signal shown in Figure 3.10, where the low frequency noise was around $10^2 \mu\text{V}/\text{m}$. The low frequency noise in this plot should be higher because the simulated DC signal being placed in the water was in the lower frequency bandwidths. The roll off that was present in this plot also corresponded to the duration of the signal in the electric field plot.

The duration of the pulse in Figure 3.11 was approximately 2.5 seconds which corresponded to the roll off that begins at 0.4 Hz in the amplitude spectral density plot. This, along with the remainder of this test set, was a good indication that the sensors were function well as far as measuring low frequency DC sources.

3.1.3 - SFOMC Offshore Tests

Two days of offshore testing were performed from August 15th, 2016 through August 19th, 2016. These tests were conducted to determine the progress and status of the electric field sensors being developed at the UI. The first test was conducted Wednesday, August 17th and the second test was conducted Friday, August 19th.

Testing on Wednesday provided a few obstacles that led to less data being collected than was desired. The driver of the source boat was inexperienced and this led to many poor runs over the course of the day. The sensors also were soaked in water from in the bay which did not have the same conductivity as the water offshore. This led to the sensors taking longer to stabilize which caused more drift in our measurements. The water was also very rough which made set up and staging between each run take much longer than normal. Because of these factors, there was only a handful of runs that were useful to analyze from Wednesday's test.

These issues were not a factor for Friday's test. The Parker driver was experienced and the weather was clear and gave us no issues. We also obtained a bucket of water from offshore to soak our sensors in before our testing on Friday.

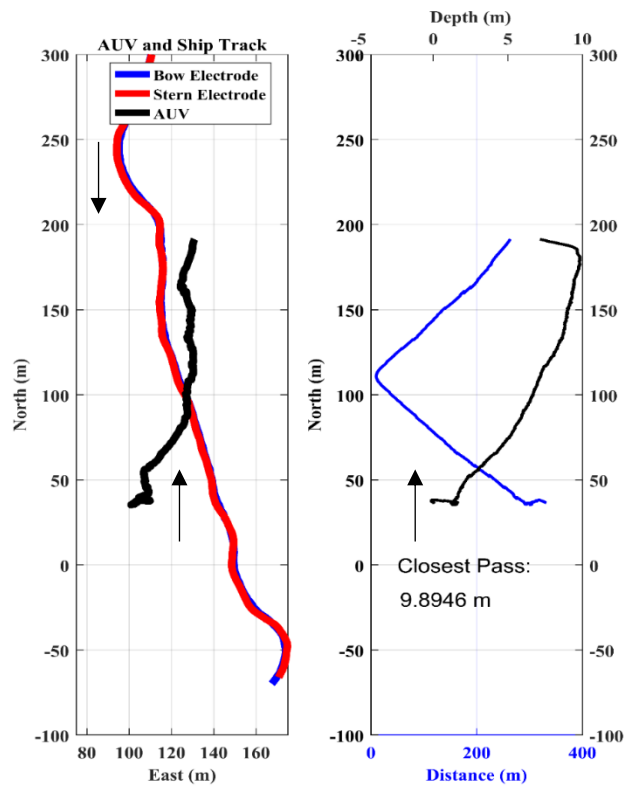


Figure 3.13: Position, depth, and closest pass of AUV and Parker for AUV 7 run 38 on Wednesday, August 17, 2016

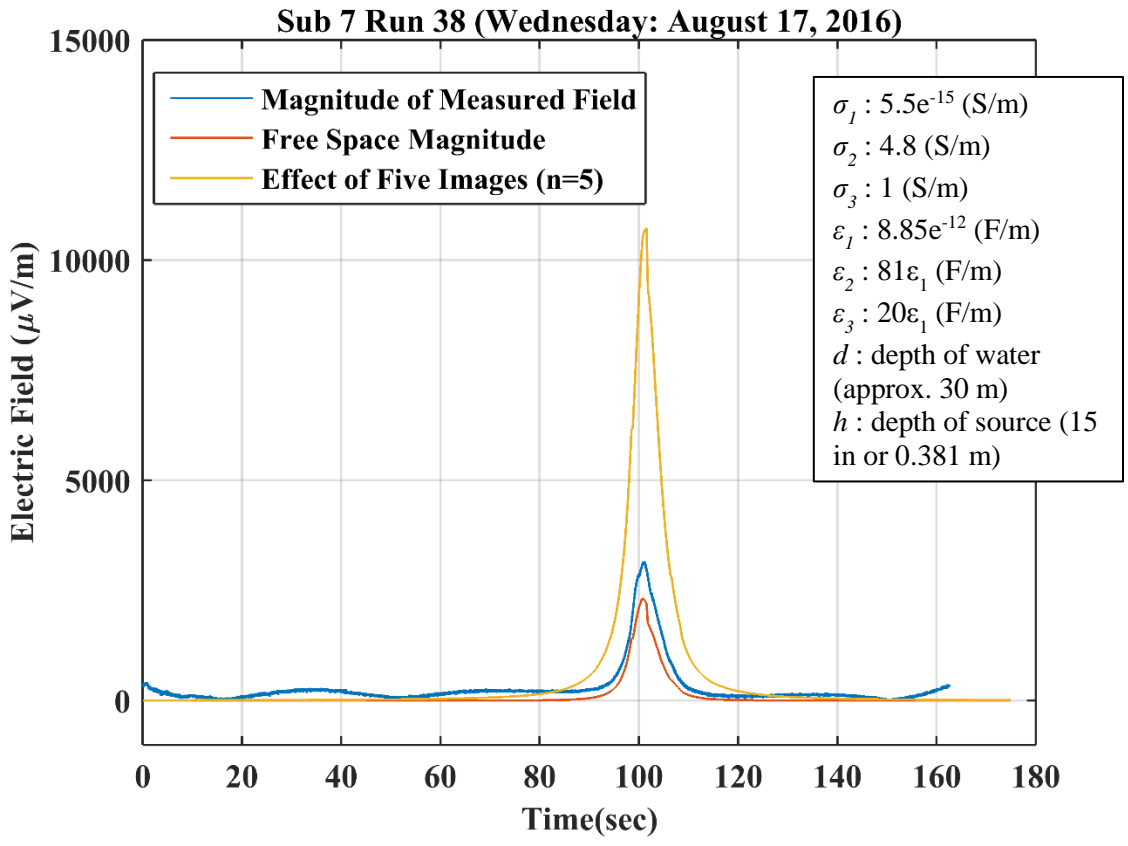


Figure 3.14: Magnitude of measured electric field for AUV 7 Run 38 Wednesday, August 17, 2016

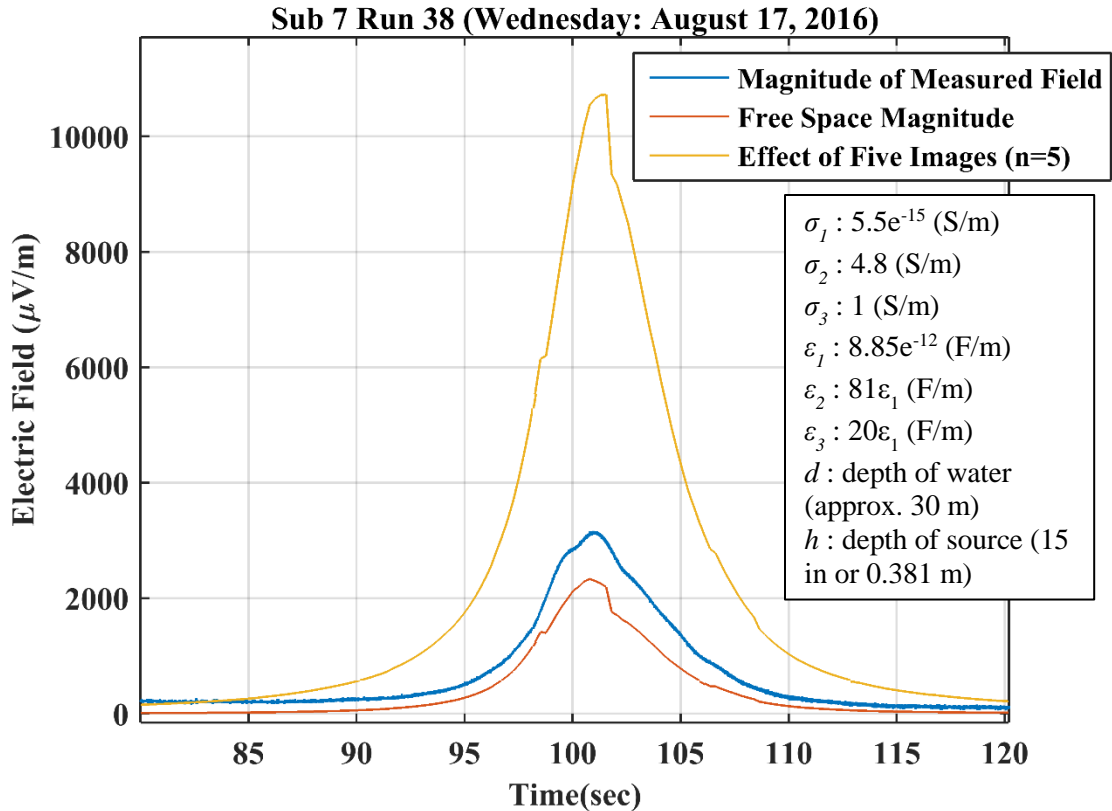


Figure 3.15: Zoomed in view of the magnitude of the measured signal from the source boat

Figure 3.13, Figure 3.14, and Figure 3.15 show a run from these tests (See Appendix for more runs). These figures show a couple things that were important to be aware of. The left plot on Figure 3.13 shows the position of the Parker boat and the AUV as they move through the run. The position data of the Parker comes from two GPS units that were placed directly above each electrode with an accuracy of approximately less than 10cm. The electrodes on the Parker were the blue and red tracks on the plot. The plot on the right of Figure 3.13 shows both the depth of the AUV in black as well as the distance between the AUV and the source on the Parker in blue. This takes into account the depth as well as North and East position of the AUV.

Figure 3.14 shows the magnitude of the measured electric field from this run along with the theoretical models of the free space electric field and the electric field including boundary effects relative to the position data for this specific run. The free space electric field model

used the position data from both the Parker and the AUV to model what the magnitude of the electric field should look like. The boundary effects were also calculated from the position data. This gives us an idea of what the predicted electric field should look like. Figure 3.14 shows a measured electric field that was close to the modeled free space field, peak values of approximately $3,000 \mu\text{V/m}$ compared to $2,500 \mu\text{V/m}$. The model with boundary effects estimated a peak value of approximately $12,000 \mu\text{V/m}$. For this run, the AUV at its closest point to the source, was a distance of 9.89 meters away. This figure shows that the measured electric field was close to the predicted free space field.

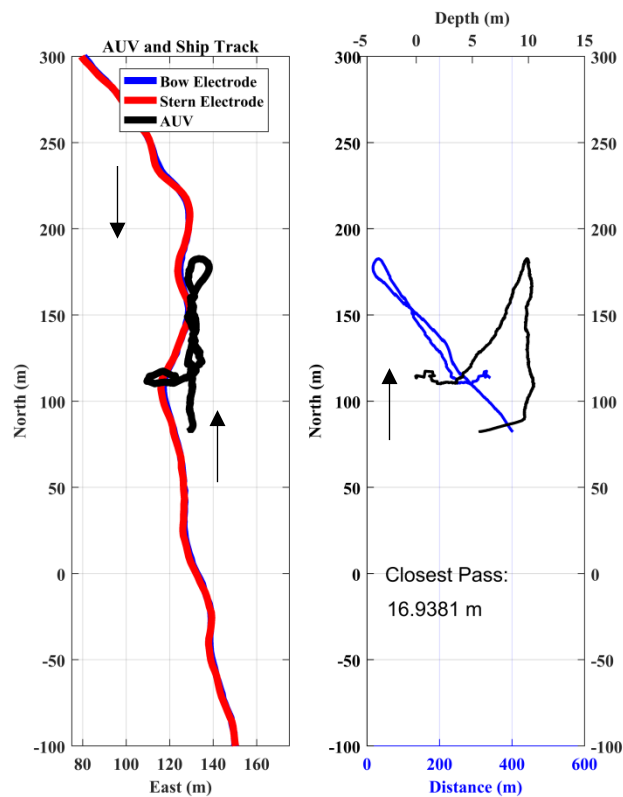


Figure 3.16: Position, depth, and closest pass of AUV and Parker for AUV 7 run 29 on Wednesday, August 17, 2016

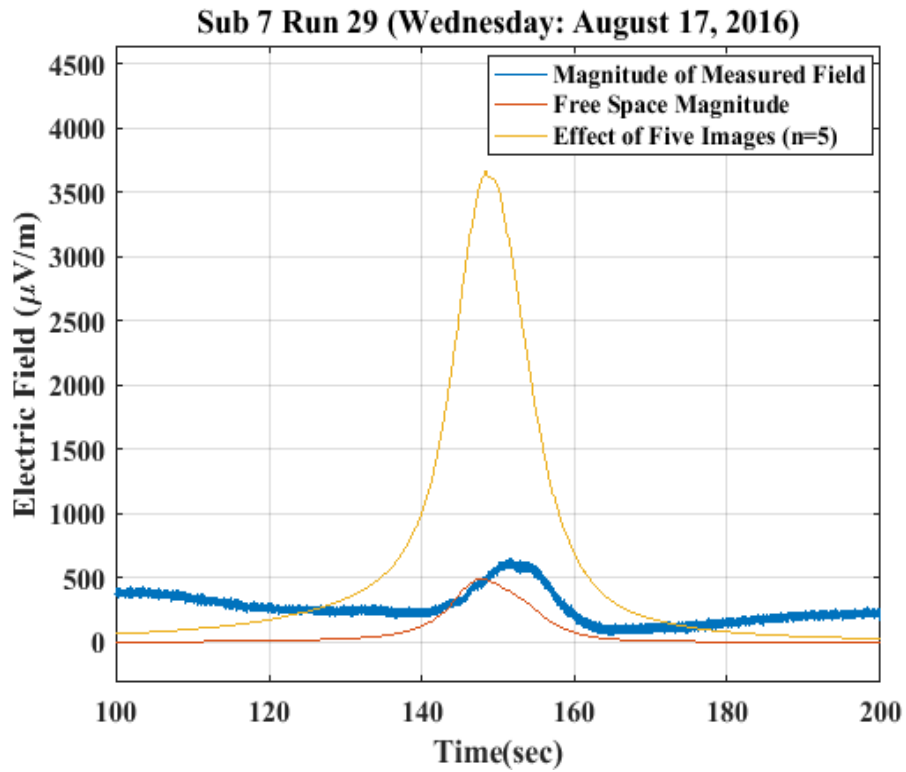
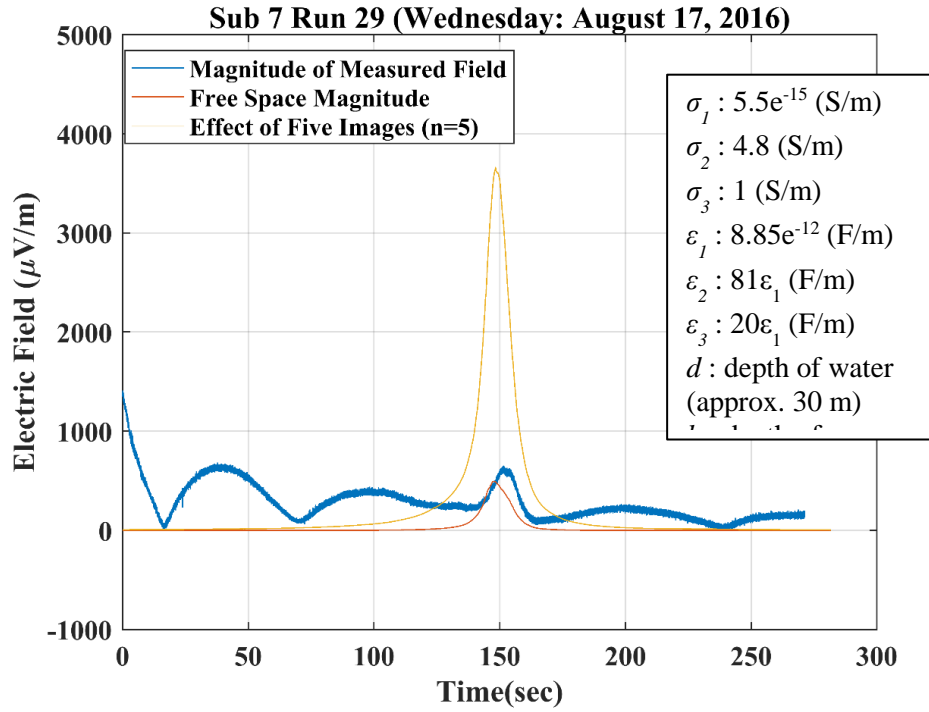


Figure 3.16, Figure 3.17, and Figure 3.18 show another run from Wednesday. This run was not one of our best runs from the day. The position plot shows that the AUV was running a different mission than the previous run. The AUV dove underwater, ran for a while and then turned around to come back to the starting point of the mission. This did not end up being more successful than our straight runs where the AUV was only going one direction. The AUV's closest pass during this run was 16.938 meters. This is getting close to doubling the distance of the closest pass of the straight missions. As seen in Figure 3.17, the peak electric field measured during this run, under $1,000 \mu\text{V}/\text{m}$, was much weaker than run 38, which was almost $3,000 \mu\text{V}/\text{m}$.

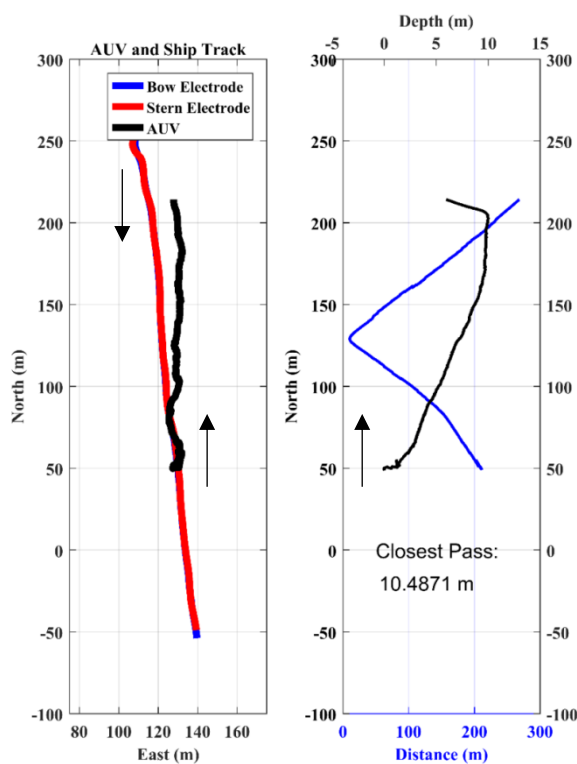


Figure 3.19: Position, depth, and closest pass of AUV and Parker for AUV 7 run 12 on Friday, August 19, 2016

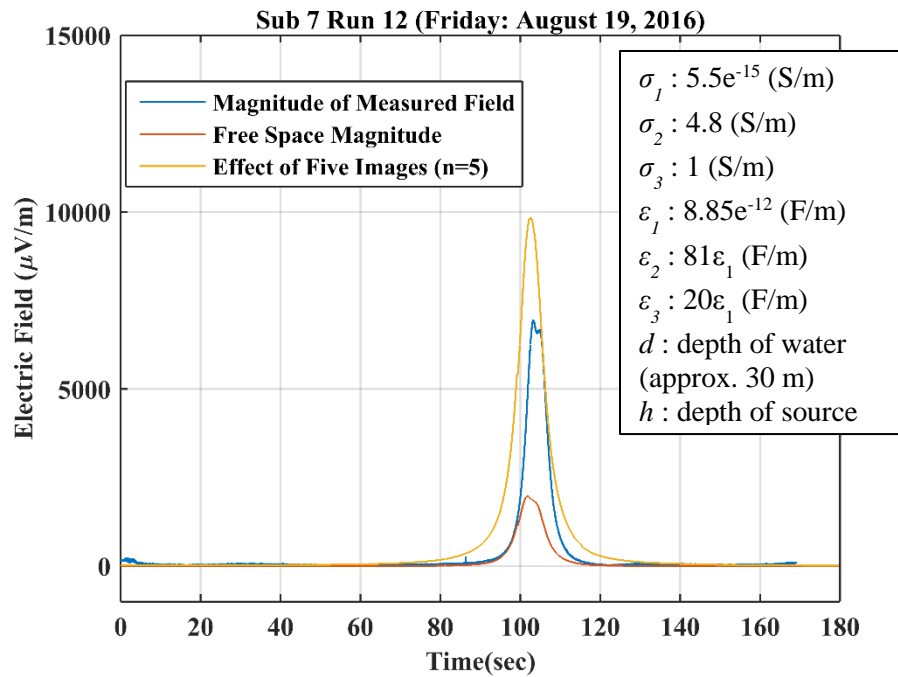


Figure 3.20: Magnitude of measured electric field for AUV 7 Run 12 Friday, August 19, 2016

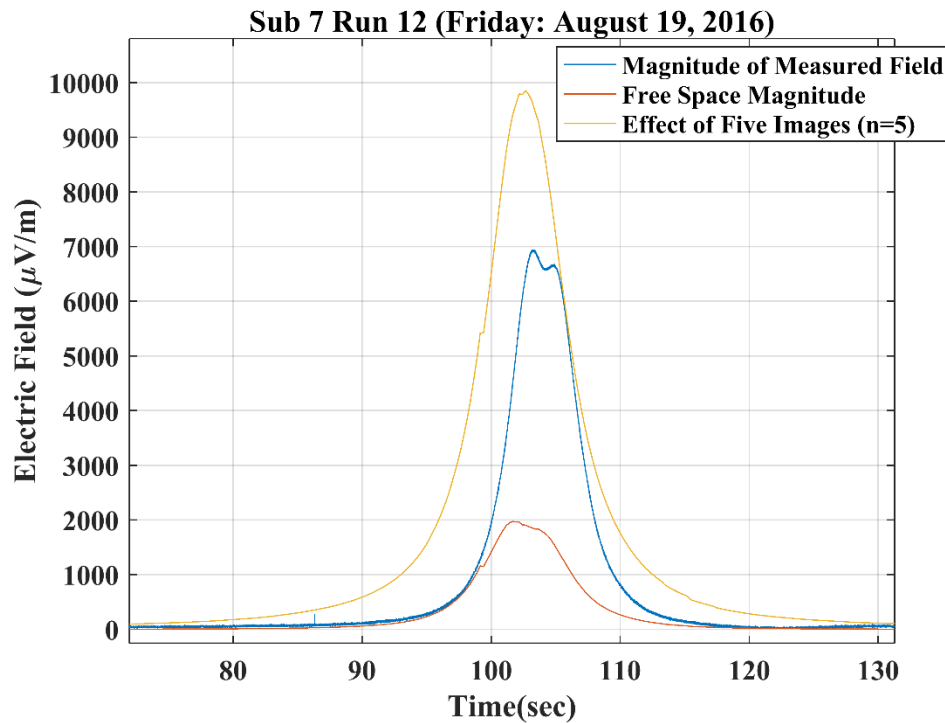


Figure 3.21: Zoomed in view of the magnitude of the measured signal from the source boat

These plots, Figure 3.19, Figure 3.20, and Figure 3.21, show one of the best runs from Friday. The position of the AUV and Parker were relatively in line with each other, and the closest pass was 10.487 meters. The magnitude of the measured electric field was in between the predictions for the free space model and the model of the boundary effects. The measured peak electric field was just under 7,000 $\mu\text{V/m}$ which was below the level of the boundary effects model, 10,000 $\mu\text{V/m}$, and above the free space model, 2,000 $\mu\text{V/m}$. We obtained a clear measurement of the electric field when the conditions were close to ideal. This allowed us to get a clear picture of the measurement capabilities of our sensor system. The following plots, Figure 3.22 and Figure 3.23, show a run from Friday with less than ideal conditions.

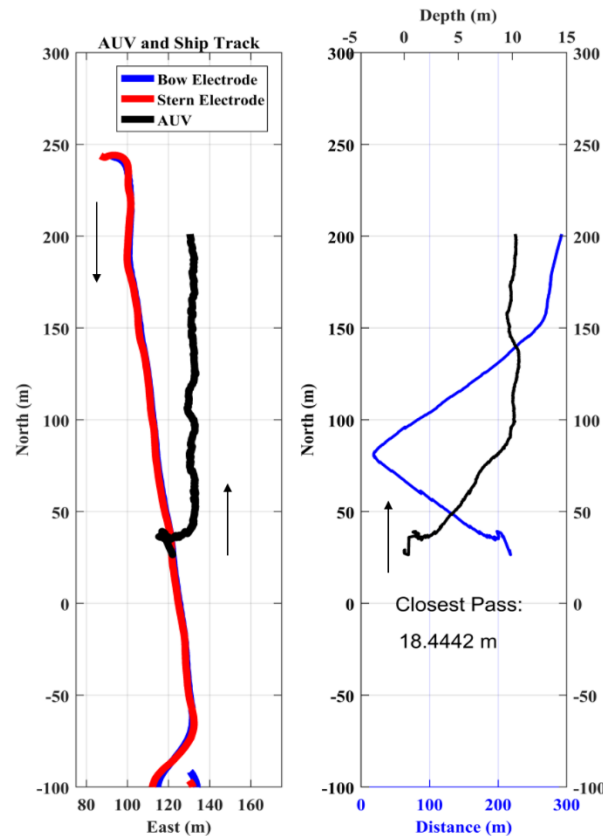


Figure 3.22: Position, depth, and closest pass of AUV and Parker for AUV 7 run 81 on Friday, August 19, 2016

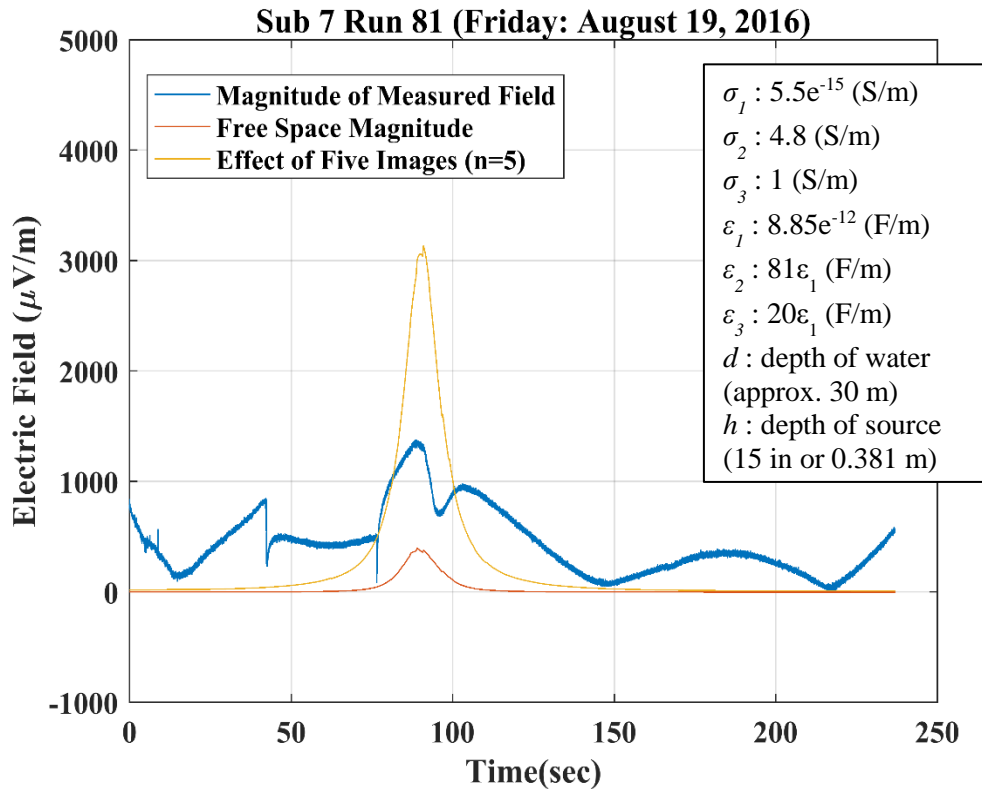


Figure 3.23: Magnitude of measured electric field for AUV 7 Run 81 Friday, August 19, 2016

For this run, the closest pass was 18.444 meters, which was almost double our goal. Ideally the AUV was running at a depth of 10 meters and would run directly under the Parker. Figure 3.22 shows that at the start of the run, the alignment was ok, but by the middle of the run when the AUV and Parker were supposed to pass, they were not close to each other. This showed up in the measurement of the electric field which could be seen in Figure 3.23. First, the measured field is relatively weak and seems to jump around. The strength of the measurement was tied in part to how close the sensor was to the outputted signal. Being farther away, the measurement was not as strong or as accurate as other runs that were more in line with the desired path.

Most of the conclusions and discussion about the results of these tests will be about runs that were similar to Figure 3.20. This plot gives a good view of how most of our better runs turned out. Looking at the difference between the free space magnitude and what was measured would indicate that there was something that was not being accounted for. This difference was much smaller when boundary effects were taken into account. It was reassuring that the actual magnitude of the measured electric field was somewhere in between these models. This helps to create a boundary of what we would believe as an accurate or valid measurement. If a measurement were to be seriously outside these model predictions, there would need to be further evaluation of what could have caused the measurement to be outside of the predicted theoretical values.

Comparing these two runs, Figure 3.20 and 3.23, showed two relatively different signal strengths. Both of these runs were ideally supposed to be set up and conducted in the same way. Because of the obstacles mentioned previously on Wednesday, we did not measure as strong of a signal as on Friday. This seemed to be rectified on Friday when the AUV and Parker were more in line during the runs and the sensors had soaked in water from offshore to come to a more stable equilibrium. Both test days produced useful data, but Friday produced more reproducible runs.

Evaluating these runs brought about some confidence in our measurement capabilities. Looking specifically at our run from Friday we saw that our measured signal was between the model of our electric field in free space and the model of our electric field with the effects of the air and seafloor boundaries. Even on Wednesday when the conditions were not ideal, our measurements were still within the modeled predictions. Because of these results and analysis,

we felt it was important to determine where possible errors could come from so that we could improve our analysis and understanding of the measurements.

3.1.4 - Sensitivity Analysis

The goal of obtaining the most accurate measurements possible included evaluating various aspects of the testing process. Being able to evaluate the testing process after the tests had been conducted was important to evaluate where possible errors could have originated. One of the biggest sources of possible error in calculating and measuring the electric field came from the navigation data from the AUV. The AUV's position was only known to within one meter at best; we evaluated how much this difference could affect the theoretical electric field. The following figure shows an evaluation of the theoretical electric field with the position of the AUV being varied in each coordinate by a meter. The depth (Z), east position (Y), and north position (X) were the coordinates that were varied by a meter (i.e. $X-1$ or $X+1$ etc.) shown in Figure 3.24.

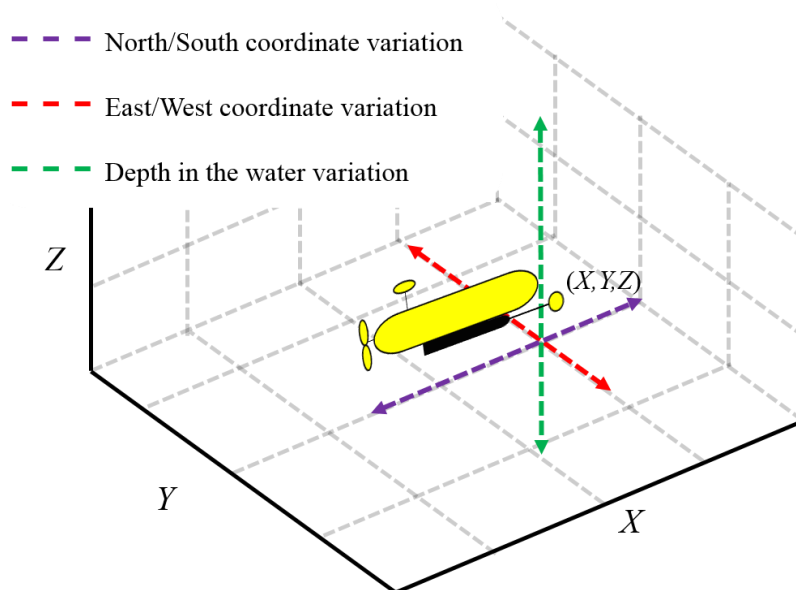


Figure 3.24: Variation of AUV position

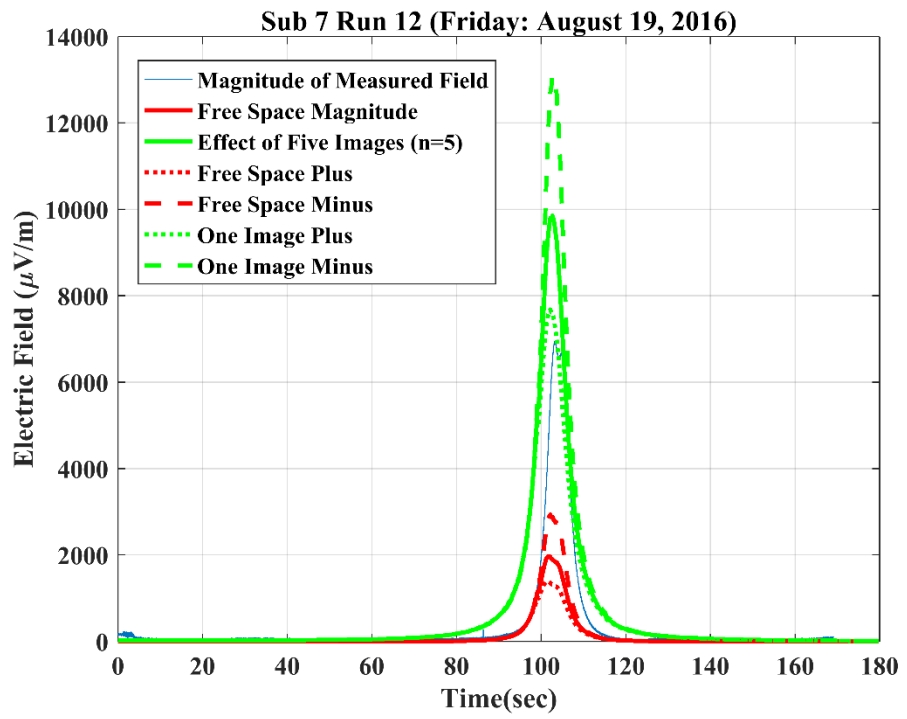


Figure 3.25: Evaluation of the sensitivity of the AUV position data on the theoretical electric field

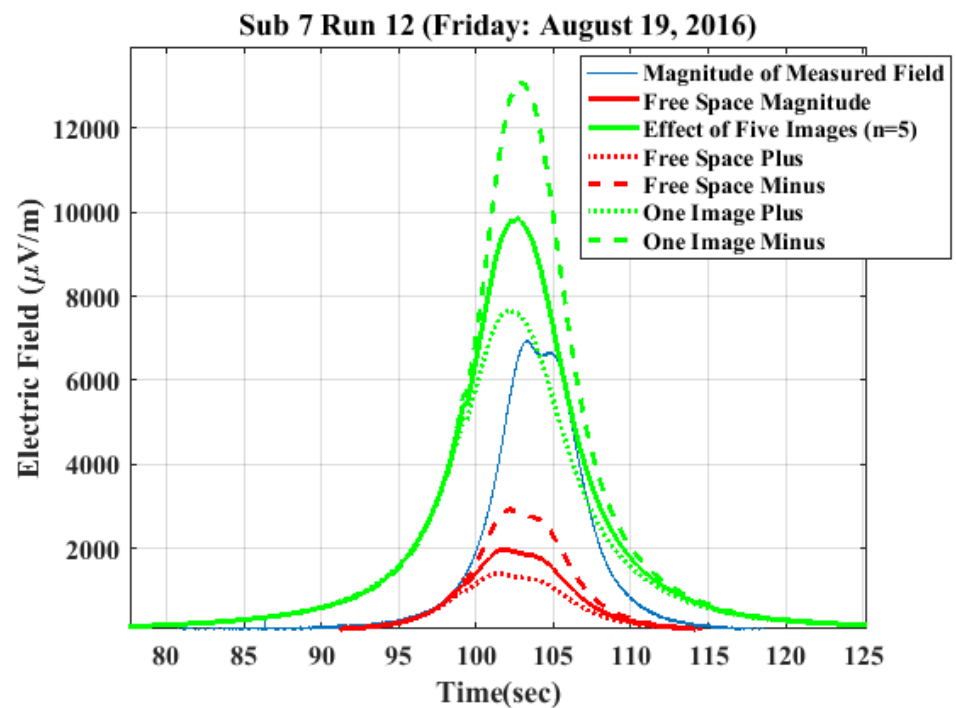


Figure 3.26: Zoomed in view of sensitivity variation

Figure 3.25 and Figure 3.26 show run 12 that was discussed in section 3.1.3. The dotted and dashed lines show what the theoretical field would look like if a meter was added or subtracted from the position of the sub. A meter was added or subtracted to each coordinate of the AUV's position. These positions were the depth and the North and East position. By adding or subtracting a meter from these coordinates, we can see how the magnitude of the theoretical electric field changes. If we take a meter away, meaning the AUV was closer to the source, the theoretical electric field reaches a value of approximately 13,000 $\mu\text{V}/\text{m}$ which was stronger than the actual position of the AUV (just under 10,000 $\mu\text{V}/\text{m}$). If we add a meter, the theoretical electric field reaches a magnitude of 7,700 $\mu\text{V}/\text{m}$, which was weaker than the theoretical electric field from the actual position data. The measured electric field peak value was very close to the predicted value of the boundary effects model when a meter was added to each coordinate. As we move the AUV closer to the source, the theoretical electric field gets stronger. The opposite was also true as we moved the AUV further from the source. This physically seems to make sense and gave us an idea of how important having accurate position data was to accurately determine the electric field. This evidence shows that the discrepancy between the measured electric field and the modeled electric field could be in part due to the navigation accuracy. The sensitivity of other factors was being investigated as well.

Chapter 4: Conclusions and Future Work

4.1 Conclusions

This project has shown progress and positive results related to the goals of the research. Testing, both in the lab and in the field, has proven the ability of the sensor system to measure electric fields within reasonable bounds. The sensor system could now be further evaluated and improved upon with the current state of the project. A plan for further research and development of the sensor and analysis of measurements can now be implemented based on this work.

Section 3.1.1 discussed how moving the preamplifier inside the sensor mold improved our measurement noise both in the lab and in the field. By implementing this change, our RMS measurements of noise went from approximately $15 \mu\text{V}/\text{m}$ to almost $1 \mu\text{V}/\text{m}$, which was right where we wanted our noise floor to be. This led to an improved noise floor which allowed for clear measurements in our field testing.

Section 2.7.2 discussed the first set of testing conducted in Florida off the side of the pier. These tests showed our ability to measure known ac and dc signals that were placed in the water. We clearly measured both 1 Hz and 10 Hz sine waves that were placed in the water. We also measured the simulated dc field that was placed in the water. We measured where in the run the source appeared as well as being able to correlate the 0.4 Hz roll off in the amplitude spectral density plot with the width of the measured source.

Section 3.1.3 discussed the ability of our sensor to operate under a moving source and measure the electric field being placed into the water. We also utilized an electric field model to evaluate our measurement and compare it to the predicted models. During the run shown in Figure 3.20, the peak of the measured electric field was approximately $7,000 \mu\text{V}/\text{m}$ which was

below the boundary effects prediction model that was at 10,000 $\mu\text{V}/\text{m}$. Our measured electric field was also above the free space electric field prediction model of approximately 2,000 $\mu\text{V}/\text{m}$. This showed that what we measured was near the bounds of our models. It was also shown in Figure 3.17 that the position of the AUV relative to the source was important in obtaining a strong measurement of the electric field. During this run, the AUV was almost twice as far away from the source as was desired. The electric field measured during this run was under 1,000 $\mu\text{V}/\text{m}$ which was much weaker than similar runs when the AUV was closer to the source.

This led to evaluating the possible error that could come from inaccuracy in AUV position measurements. Section 3.1.4 discussed how the predicted models changed when the position of the AUV changed. This evaluation showed that if we add or subtract a meter to the position of the AUV, the predicted values change by approximately 3,000 $\mu\text{V}/\text{m}$ in either direction which meant the measured electric field peak value was just outside these error bounds. This shows a boundary that can be developed based on the accuracy of the AUV position. This gives confidence that the measured field can be improved with more accurate AUV position data.

4.2 Future Work

There will be further development of the sensor system that will continue to take place. Analysis of the AUV position data could be an area that leads to greater accuracy in measuring electric fields. Further analysis of the prediction models will help with this endeavor. The final hardware and design for the sensor system was still being developed at the time of this writing.

References

- [1] S. C. Constable, A. S. Orange, G. M. Hoversten, and H. F. Morrison, "Marine magnetotellurics for petroleum exploration Part I: A sea-floor equipment system," *Geophysics*, vol. 63, no. 3, pp. 816-825, 1998.
- [2] S. R. Qualls *et al.*, "Underwater electric potential measurements using auvs," in *OCEANS'15 MTS/IEEE Washington*, 2015, pp. 1-4: IEEE.
- [3] C. Walker, "Magnetic Signature Mapping of a Moving Ship Using a Fleet of Autonomous Underwater Vehicles," University of Idaho, 2012.
- [4] R. A. Oare, "Developing a Low-Noise Data Acquisition System for Detection of Electric and Magnetic Fields in Seawater," University of Idaho, 2016.
- [5] Z. Wang, M. Deng, K. Chen, and M. Wang, "An ultralow-noise Ag/AgCl electric field sensor with good stability for marine EM applications," in *Sensing Technology (ICST), 2013 Seventh International Conference on*, 2013, pp. 747-750: IEEE.
- [6] R. T. Rebich, J. L. Young, C. L. Wagner, and R. G. Olsen, "Comparison of the up-over-down approximation with the quasi-electrostatic approximation for ELF fields in layered media," in *Antennas and Propagation (APSURSI), 2011 IEEE International Symposium on*, 2011, pp. 2371-2374: IEEE.
- [7] S. Pawar, P. Murugavel, and D. Lal, "Effect of relative humidity and sea level pressure on electrical conductivity of air over Indian Ocean," *Journal of Geophysical Research: Atmospheres*, vol. 114, no. D2, 2009.
- [8] R. Cox, M. McCartney, and F. Culkin, "The specific gravity/salinity/temperature relationship in natural sea water," in *Deep Sea Research and Oceanographic Abstracts*, 1970, vol. 17, no. 4, pp. 679-689: Elsevier.
- [9] R. E. Boyce, "Electrical resistivity of modern marine sediments from the Bering Sea," *Journal of Geophysical Research*, vol. 73, no. 14, pp. 4759-4766, 1968.
- [10] W. Ellison *et al.*, "New permittivity measurements of seawater," *Radio science*, vol. 33, no. 3, pp. 639-648, 1998.
- [11] S. Arcone, S. Grant, G. Boitnott, and B. Bostick, "Complex permittivity and clay mineralogy of grain-size fractions in a wet silt soil," *Geophysics*, vol. 73, no. 3, pp. J1-J13, 2008.

Appendix A: August 2016 SFOMC Tests

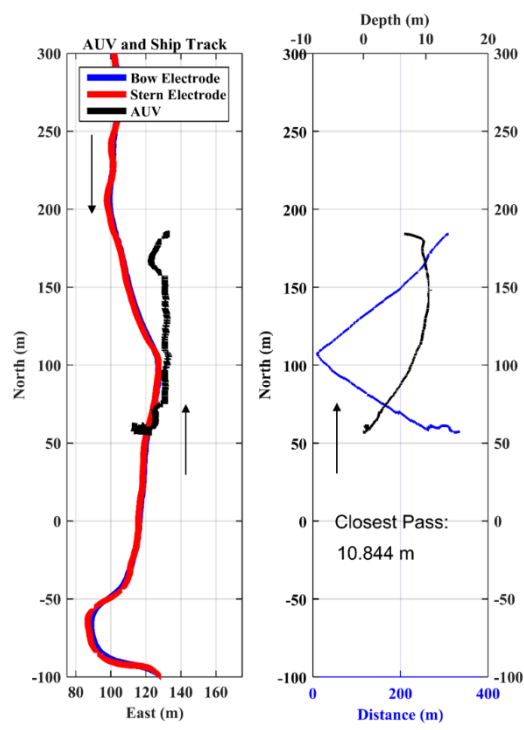


Figure A.1: Position, depth, and closest pass of AUV and Parker for AUV 7 run 36 on Wednesday, August 17, 2016

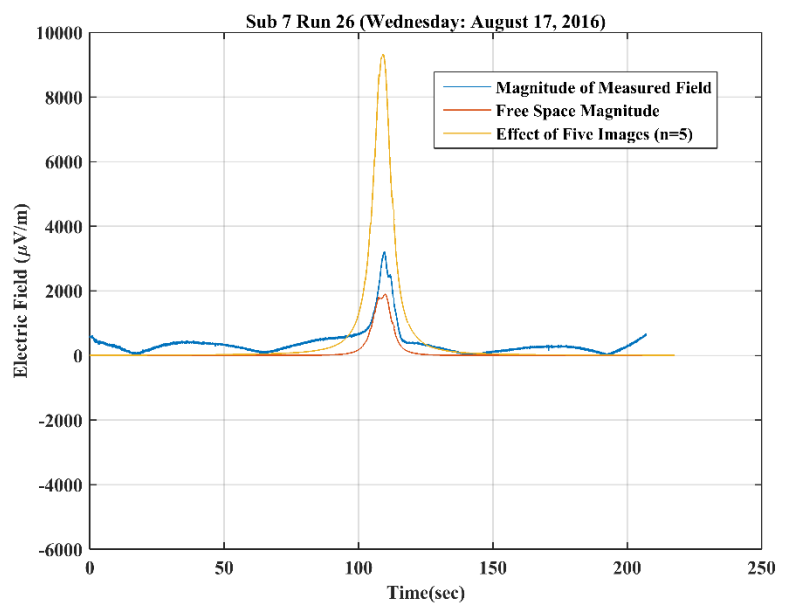


Figure A.2: Magnitude of measured electric field for AUV 7 Run 26 Wednesday, August 17, 2016

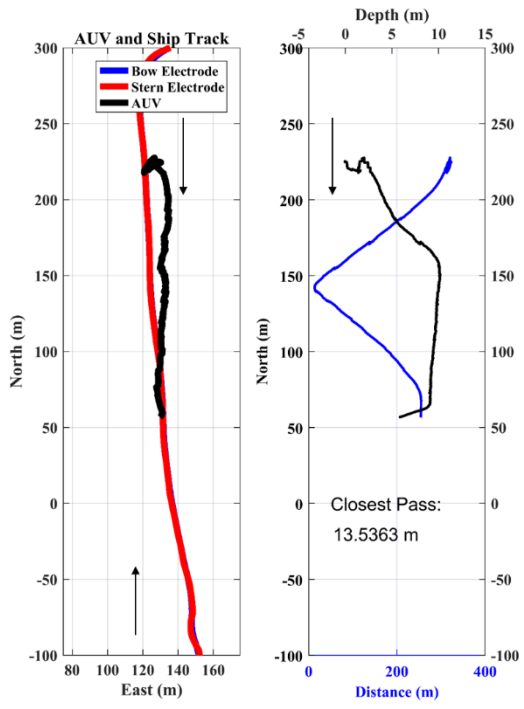


Figure A.3: Position, depth, and closest pass of AUV and Parker for AUV 7 run 03 on Friday, August 19, 2016

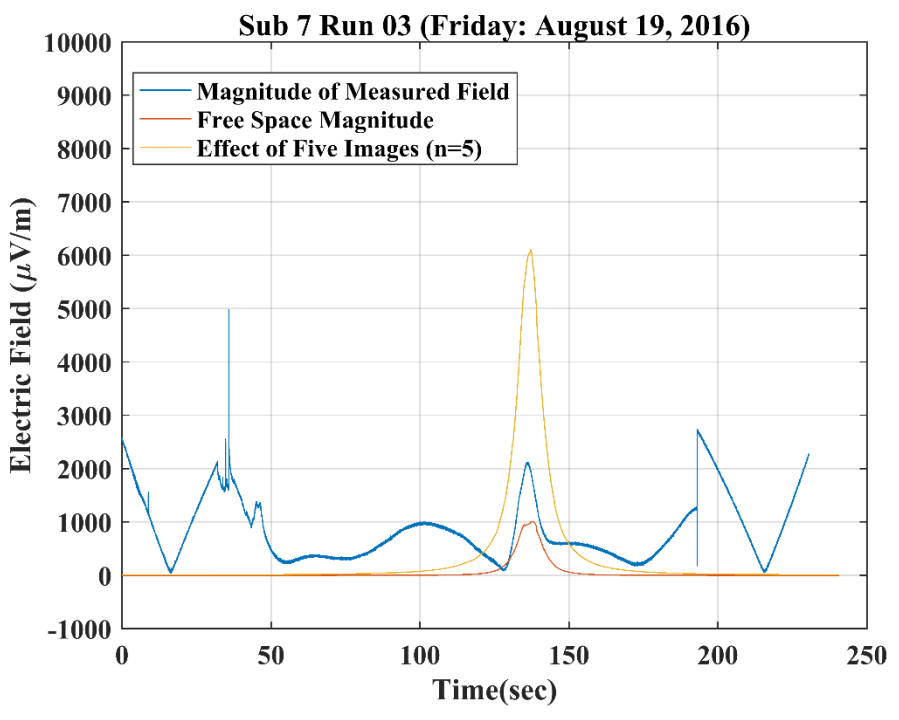


Figure A.4: Magnitude of measured electric field for AUV 7 Run 03 Friday, August 19, 2016

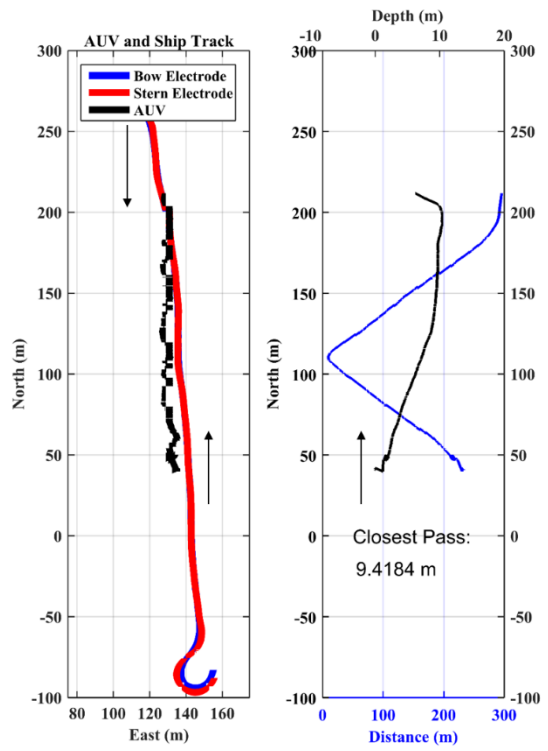


Figure A.5: Position, depth, and closest pass of AUV and Parker for AUV 7 run 06 on Friday, August 19, 2016

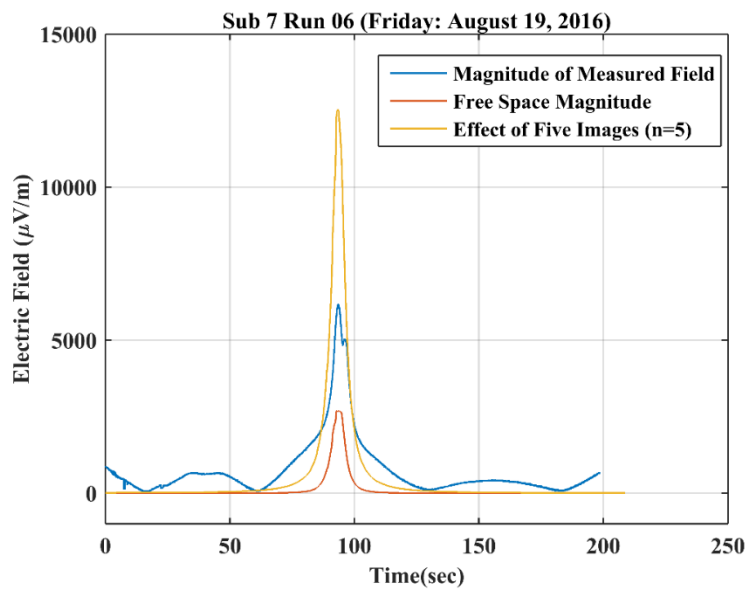


Figure A.6: Magnitude of measured electric field for AUV 7 Run 06 Friday, August 19, 2016

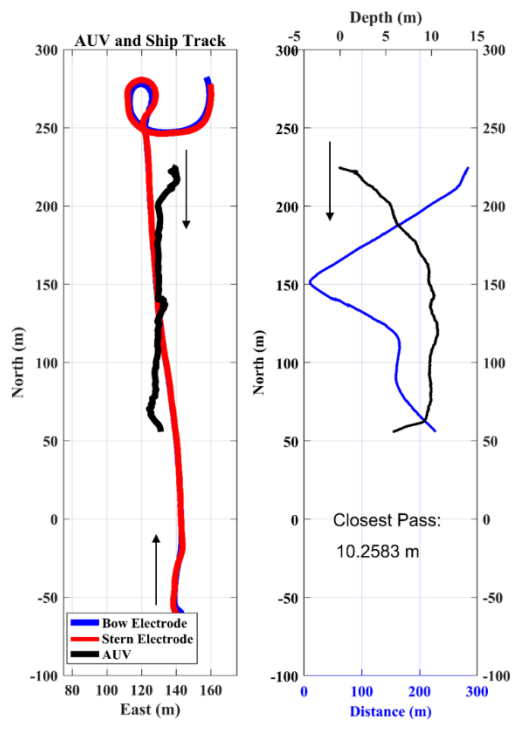


Figure A.7: Position, depth, and closest pass of AUV and Parker for AUV 7 run 09 on Friday, August 19, 2016

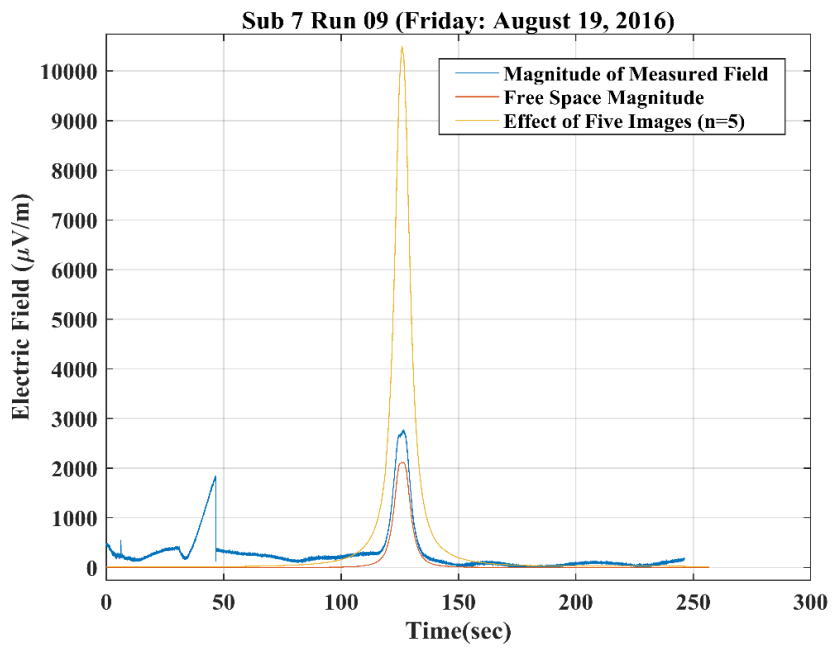


Figure A.8: Magnitude of measured electric field for AUV 7 Run 09 Friday, August 19, 2016

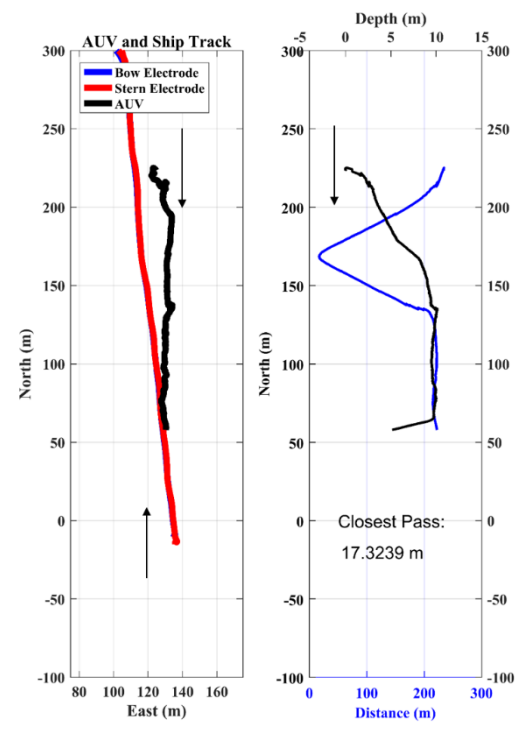


Figure A.9: Position, depth, and closest pass of AUV and Parker for AUV 7 run 16 on Friday, August 19, 2016

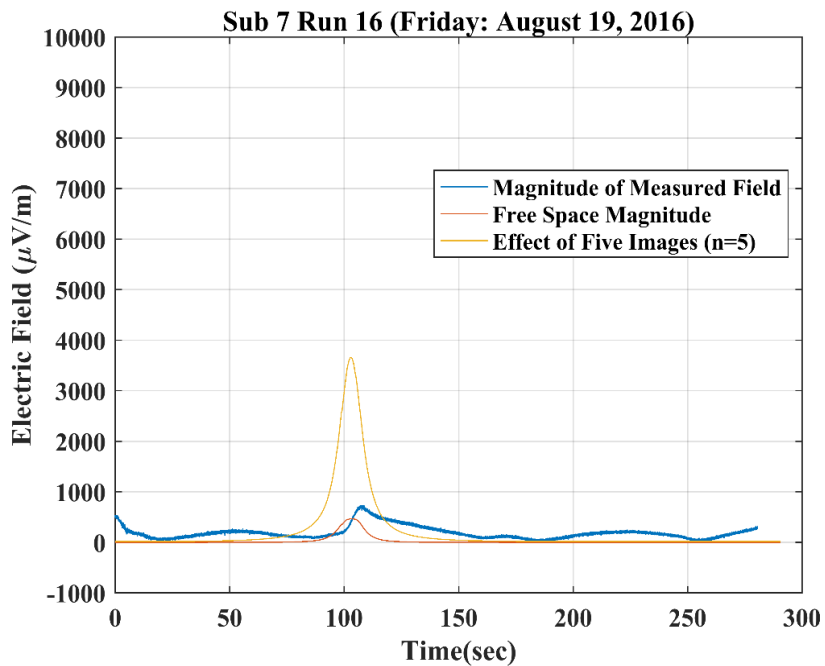


Figure A.10: Magnitude of measured electric field for AUV 7 Run 16 Friday, August 19, 2016

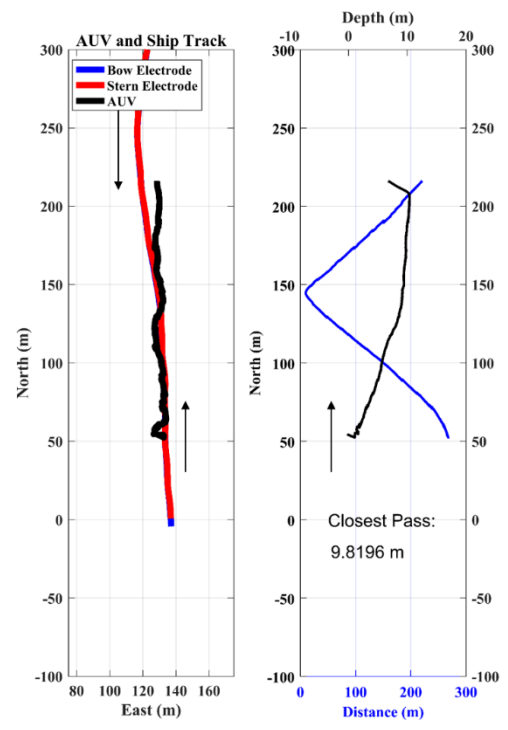


Figure A.11: Position, depth, and closest pass of AUV and Parker for AUV 7 run 19 on Friday, August 19, 2016

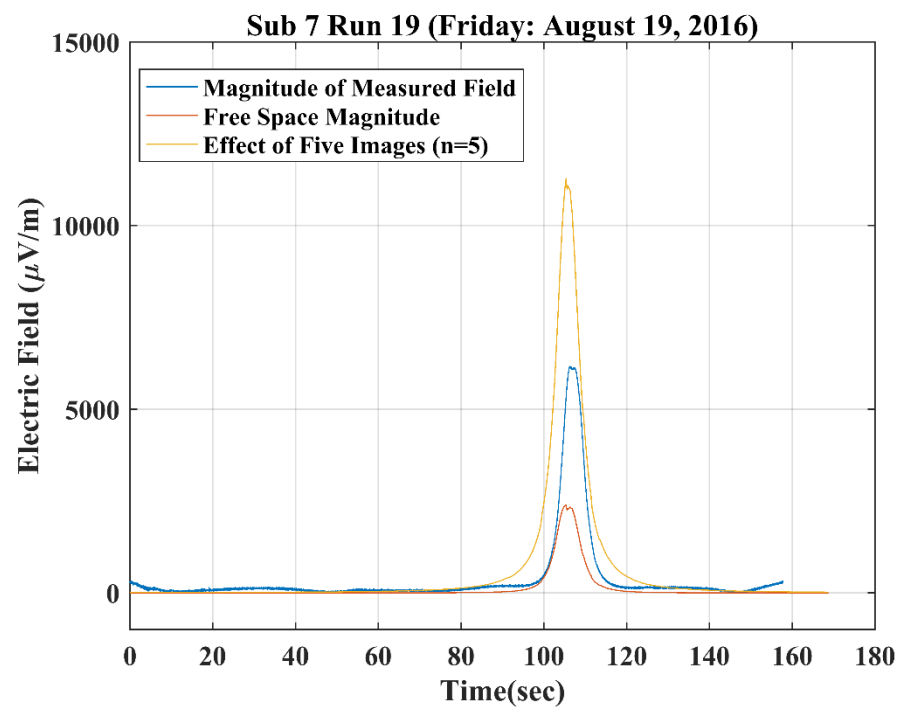


Figure A.12: Magnitude of measured electric field for AUV 7 Run 19 Friday, August 19, 2016

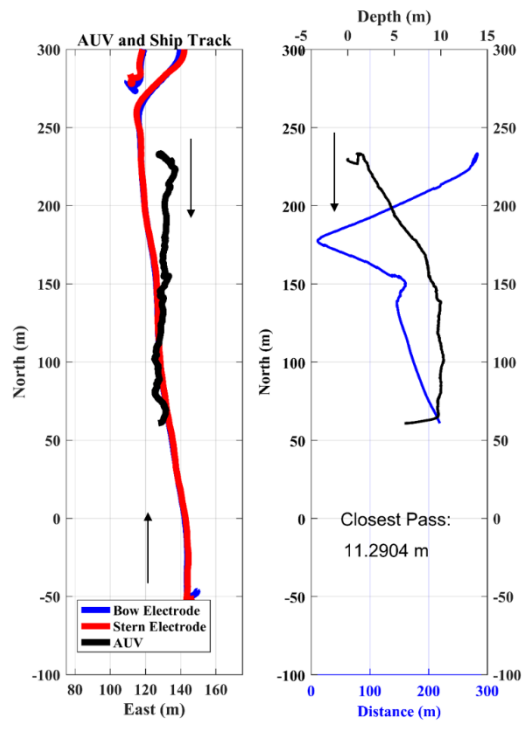


Figure A.13: Position, depth, and closest pass of AUV and Parker for AUV 7 run 22 on Friday, August 19, 2016

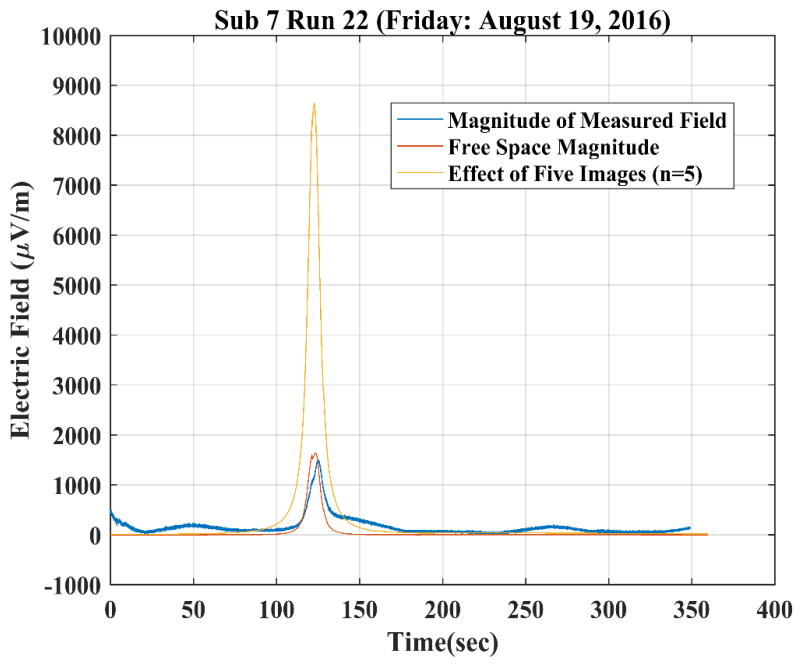


Figure A.14: Magnitude of measured electric field for AUV 7 Run 22 Friday, August 19, 2016

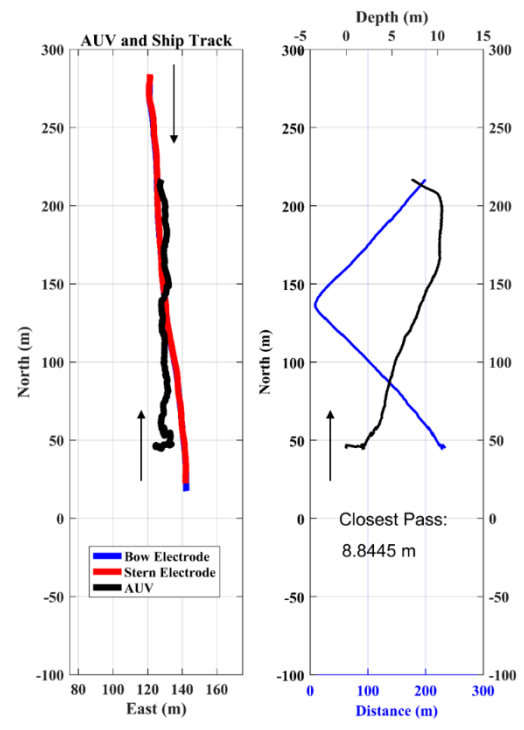


Figure A.15: Position, depth, and closest pass of AUV and Parker for AUV 7 run 25 on Friday, August 19, 2016

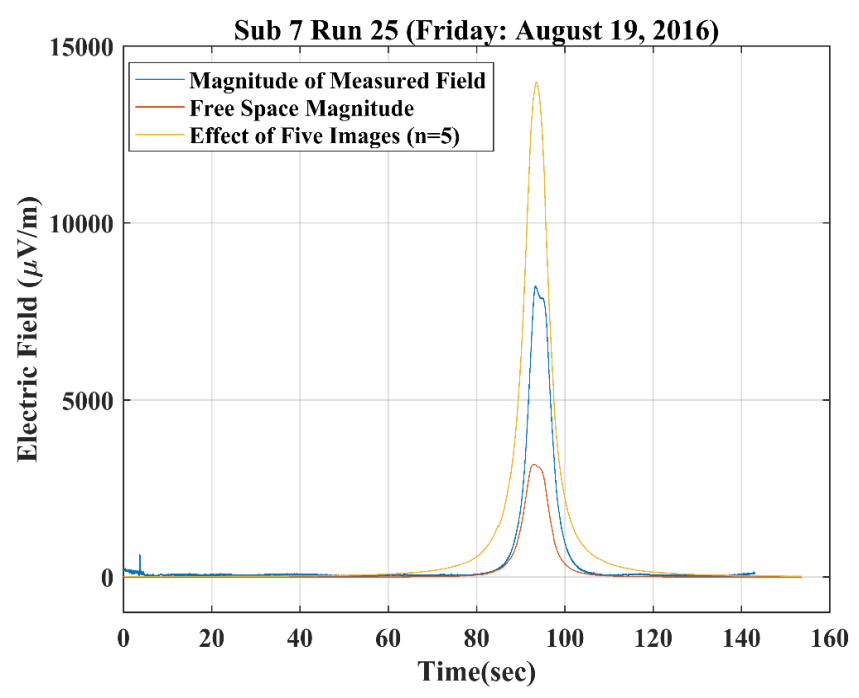


Figure A.16: Magnitude of measured electric field for AUV 7 Run 25 Friday, August 19, 2016

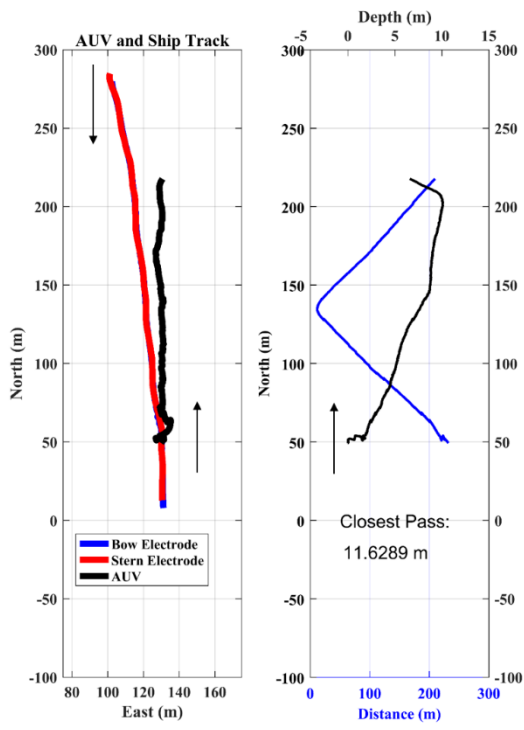


Figure A.17: Position, depth, and closest pass of AUV and Parker for AUV 7 run 31 on Friday, August 19, 2016

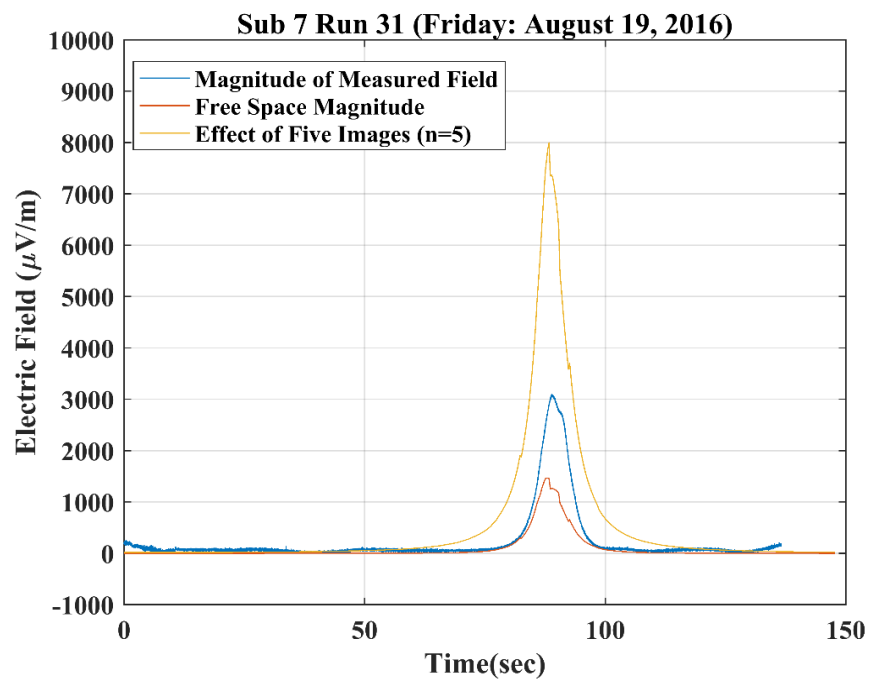


Figure A.18: Magnitude of measured electric field for AUV 7 Run 31 Friday, August 19, 2016

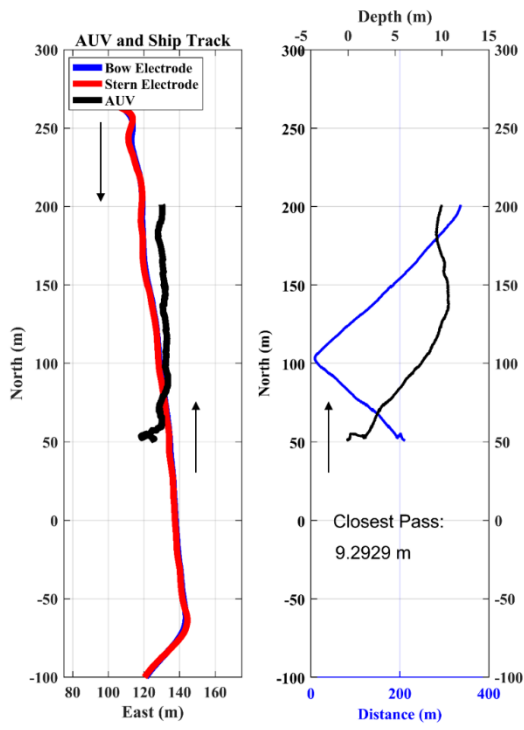


Figure A.19: Position, depth, and closest pass of AUV and Parker for AUV 7 run 73 on Friday, August 19, 2016

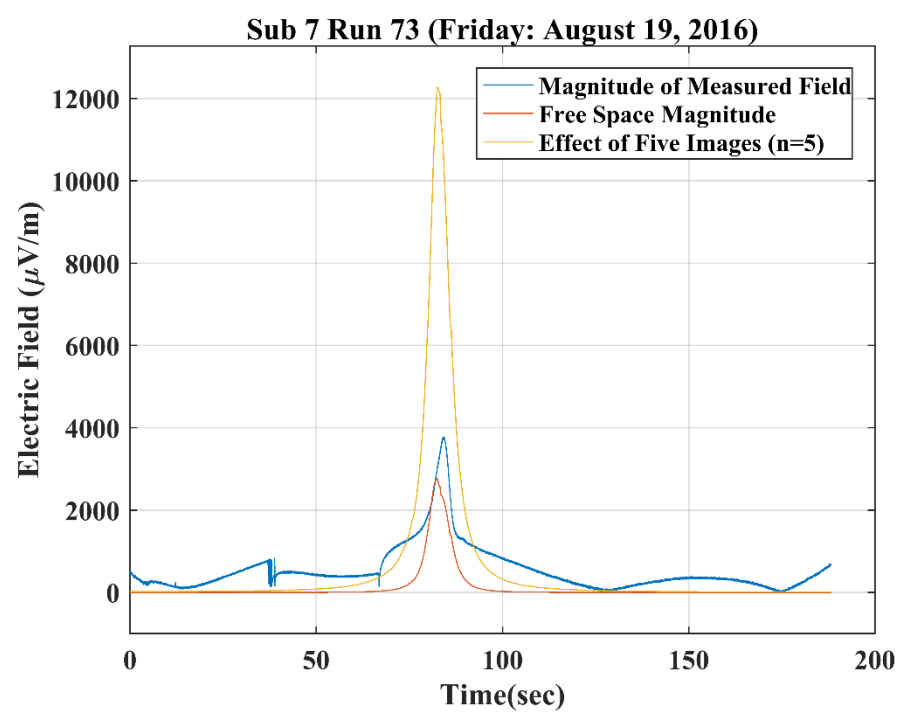


Figure A.20: Magnitude of measured electric field for AUV 7 Run 73 Friday, August 19, 2016

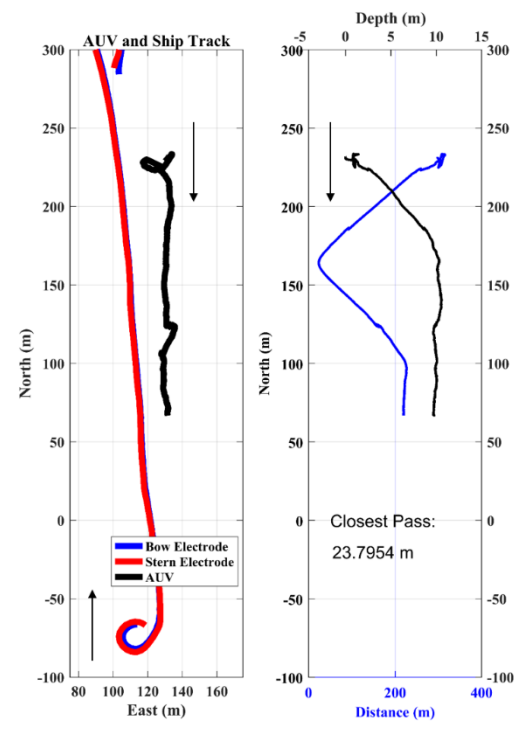


Figure A.21: Position, depth, and closest pass of AUV and Parker for AUV 7 run 75 on Friday, August 19, 2016

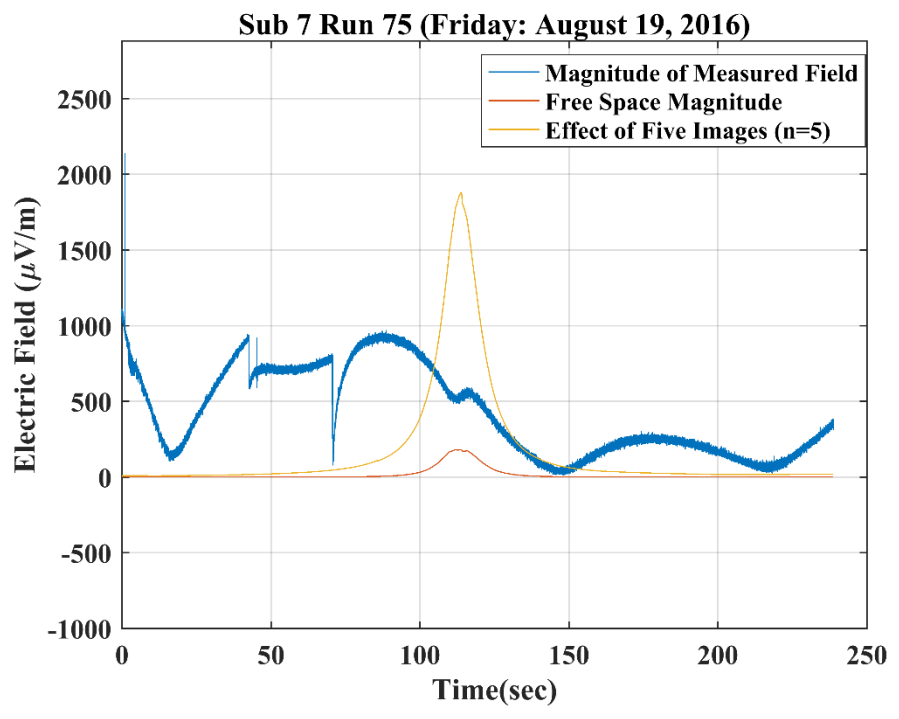


Figure A.22: Magnitude of measured electric field for AUV 7 Run 75 Friday, August 19, 2016

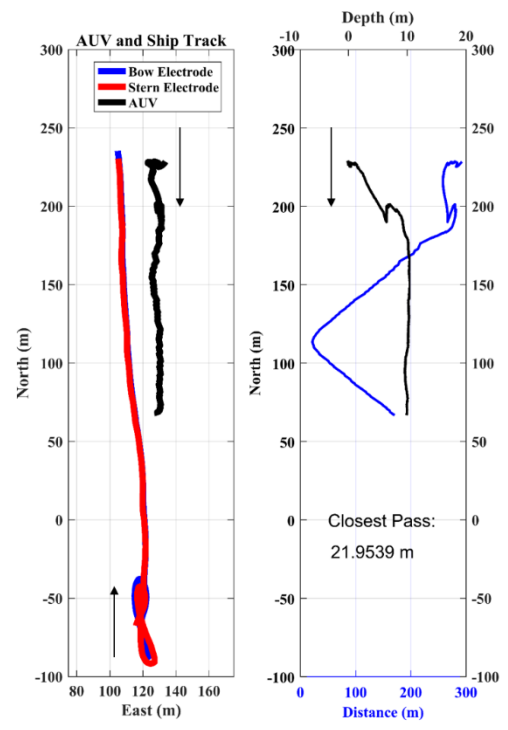


Figure A.23: Position, depth, and closest pass of AUV and Parker for AUV 7 run 79 on Friday, August 19, 2016

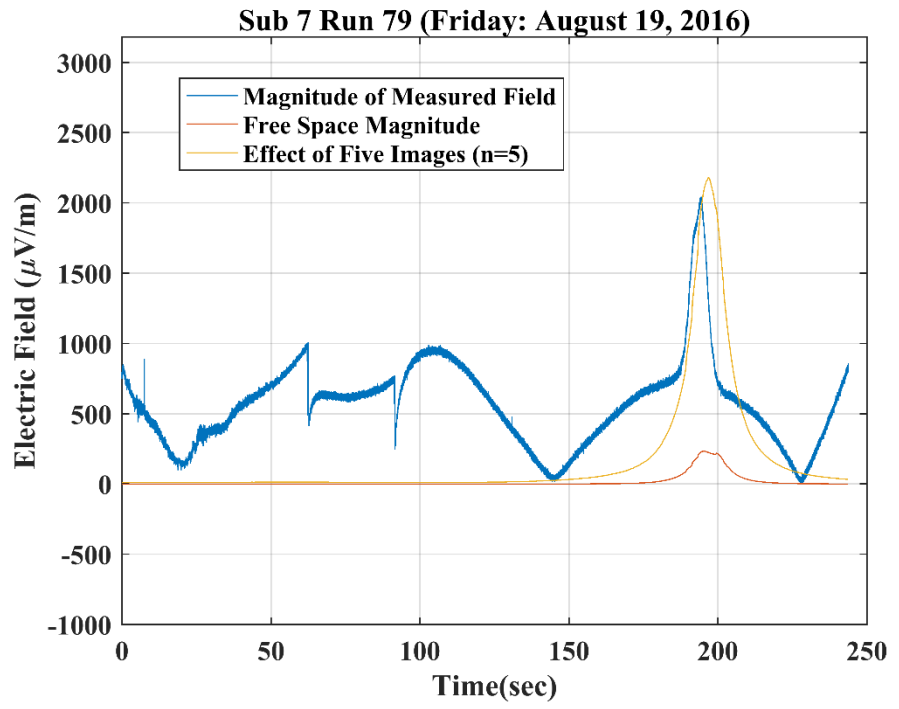


Figure A.24: Magnitude of measured electric field for AUV 7 Run 75 Friday, August 19, 2016